NPL Report DEPC-MPE 002

Performance and Durability of PEM Fuel Cells: A Review

G Hinds

September 2004

NPL Report DEPC-MPE 002

September 2004

Performance and Durability of PEM Fuel Cells: A Review

G Hinds
Engineering and Process Control Division
National Physical Laboratory
Teddington, Middlesex TW11 0LW, UK

ABSTRACT

A critical review of the literature has been undertaken to establish current understanding of the performance and durability of polymer electrolyte membrane (PEM) fuel cells. The experimental techniques employed to characterise fuel cell performance and durability are critically evaluated and the various degradation modes are discussed with reference to the literature. Key measurement issues are identified in the context of the Materials Programmes.

ISSN 1744-0262

National Physical Laboratory
Teddington, Middlesex, UK, TW11 0LW

We gratefully acknowledge the financial support of the UK Department of
Trade and Industry (National Measurement System Policy Unit)

Approved on behalf of the Managing Director, NPL,
by Dr M G Gee, Knowledge Leader, Materials Performance Team
authorised by Director, Engineering and Process Control Division

CONTENTS

1. INTRODUCTION

The depletion of fossil fuel resources, energy security, and government environmental policy represent the most significant drivers towards the development of a global hydrogen economy. The advantages of fuel cells over other sources of power are high efficiency, low emissions, modularity, fuel flexibility and high power density. The high efficiency arises from the fact that fuel cells convert chemical energy directly to electrical energy without the Carnot limitation that applies to thermal engines. The efficiency of fuel cells for generating electricity is 40%–60% and can reach 85%–90% in combined heat and power (CHP) mode, i.e. if the heat generated from the cell reaction is also used. The only waste product is pure water when hydrogen is used as the fuel. Fuel cells can be used on a micro/local level without loss of efficiency, thereby avoiding transmission losses associated with long distance power lines. The three major issues currently confronting fuel cell developers and manufacturers are cost of components, establishment of a refuelling infrastructure and durability of the systems in service. From a performance perspective the durability and sustained fitness for purpose of fuel cells are critical to their widespread commercial uptake.

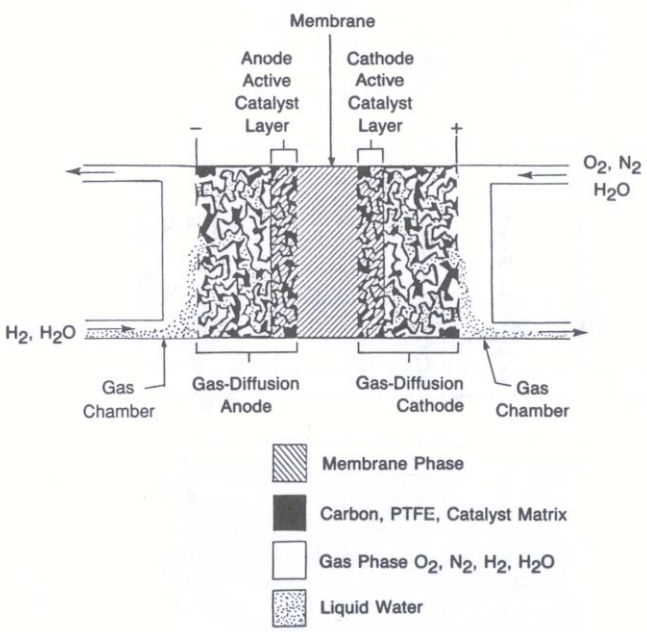

Fig. 1: Components of a PEMFC[1].

The polymer electrolyte membrane fuel cell (PEMFC) is considered the most likely candidate for transport applications due to its high power density, low operating temperature (for fast start-up), high power-to-weight ratio and absence of corrosive fluids. The technology was initially developed by General Electric in the 1960s for use by NASA on their first manned space missions. The Gemini program employed a 1 kW PEMFC stack as an auxiliary power source that also provided the astronauts with clean drinking water. The electrolyte membrane was a polystyrene sulphonate polymer that proved unstable, prompting NASA to switch to alkaline fuel cell

technology for subsequent missions. In the late 1980s Ballard Power Systems (Vancouver) and Los Alamos National Labs (California) began developing PEM fuel cells with a Nafion membrane manufactured by Dupont, which is more stable than the polystyrene sulphonate polymer. The next decade saw a dramatic decrease in electrocatalyst loading and substantially improved performance. Increased funding from the automotive sector and energy policy promoting fuel cells have positioned PEMFC cell technology on the brink of widespread commercial uptake, with most manufacturers well into the demonstration stage and some already operating in niche markets.

The various components of a PEMFC are shown schematically in Fig. 1. The fuel is supplied to the anode and the oxidant (oxygen or air) to the cathode. Hydrogen is the most common fuel, although methanol is used in a variant of the PEMFC known as the direct methanol fuel cell (DMFC)[2]. In a H_2/O_2 cell, the following reaction occurs at the anode:

$$H_2 \rightarrow 2H^+ + 2e^- \quad (1)$$

The dissociation of H_2 and adsorption of hydrogen atoms on the anode electrocatalyst leads to the formation of H^+ ions which migrate to the cathode through the proton-conducting membrane. Since the membrane is electronically insulating, the electrons are forced to flow through an external load to the cathode, thereby generating dc current. At the cathode H^+ ions, electrons and oxygen molecules combine to form water in the following reaction:

$$O_2 + 4H^+ + 4e^- \rightarrow 2H_2O \quad (2)$$

The stoichiometry of each reactant gas is an important experimental parameter in fuel cell testing. A 1:1 stoichiometry refers to the flow rate required to maintain a constant reactant concentration at the electrode at a fixed current density (reaction rate). Usually a higher stoichiometry is required at the cathode (typically 2-4) than at the anode (typically 1-2) due to the more sluggish mass transport rate of oxygen. This should not be confused with the fact that two moles of hydrogen are required for every mole of oxygen taking part in the reaction. The water produced in the cathodic reaction is removed by the excess gas stream and flooding can occur if the gas flow rate and temperature are not sufficiently high.

A comprehensive review of PEMFC design and fabrication was published by Mehta and Cooper[3].

The properties of the solid polymer membrane at the heart of the PEMFC are critical to its operation. Nafion is the most common membrane employed at present, although novel membranes are currently the subject of considerable research effort. Nafion is a derivative of PTFE, which consists of a hydrophobic PTFE backbone with hydrophilic sulphonic acid side chains. When these side chains are hydrated, the membrane can conduct protons while remaining electronically insulating, which is key to its use in PEM fuel cells. Nafion is a translucent plastic material, which is

resistant to chemical attack, a strong proton donor, transports water rapidly and can function as both a super-acid catalyst and a cation exchange membrane. Its conductivity is highly dependent on water content, which means that water management is an essential part of PEMFC operation. This is normally achieved by humidification of inlet gases. Due to the requirement for Nafion to be hydrated, membrane use is limited to below 100 °C at ambient pressure. Research into higher temperature membranes is an important developmental step in PEMFC technology. A Dow membrane also based on sulphonated PTFE but with shorter side chains and improved transport properties was developed in the 1980s. The power density achievable using this membrane was more than double that of Nafion. However most research groups continue to use Nafion due to its lower cost and ease of membrane fabrication.

On each side of the membrane is a thin layer of nanoparticulate precious metal electrocatalyst of order 10 μm in thickness. The electrocatalyst may be either unsupported as a nanoparticulate powder or supported on high surface area graphitic carbons (200 m^2 g^{-1}). Supported catalysts are typically 20-40 wt% metal with electrocatalyst loadings in the range 0.1-0.5 mg cm^{-2}. Due to the low operating temperature and acidic environment, precious metal electrocatalysts are required. Platinum is the most effective electrocatalyst known for both oxidation of hydrogen and reduction of oxygen reactions. However, the activity of platinum electrocatalysts may be severely reduced by small concentrations (> 10 ppm) of carbon monoxide (CO) in the reactant gas. This is of particular concern for systems using reformate (hydrogen processed from natural gas). For this reason the anode electrocatalyst is often a PtRu alloy, which is more resistant to carbon monoxide poisoning.

The reactant gas is fed to each electrode through a gas diffusion layer (GDL), which is typically made from carbon cloth or carbon paper. The dual function of the GDL is (a) to allow reactant gas to diffuse uniformly to the electrocatalyst layers and (b) to collect current from reaction sites. In addition, a hydrophobic phase (usually PTFE) is often added to the GDL to avoid flooding. It follows that candidate materials for the GDL must have high porosity, low resistance and low cost. The GDL must also be able to withstand compressive forces and chemical attack. The membrane together with electrocatalyst and backing layers is known as a membrane electrode assembly (MEA).

The Three Phase Boundary (TPB) is a zone in which the open pores, electrocatalyst and electrolyte are in close contact. The reaction process requires flow of protons via the electrolyte, supply of reactant gas through open pores and flow of electrons in the GDL. The active layer therefore contains an intimate mixture of electrolyte and electrocatalyst, with intermingled electronic, ionic and mass transport pathways. Diffusion of reactant through electrolyte is a significant source of mass transport limitation. The detailed mechanisms of charge transport, mass transport and electrocatalytic reaction within the TPB are not well understood.

MEA fabrication techniques are highly proprietary but usually involve mixtures of nanoparticulate precious metal, carbon and persulphonated ionomer powders which are dissolved in a solvent such as isopropanol to form an ink. The ink may be deposited directly onto the membrane[4,5] or indirectly via a decal from which the

electrode is transferred to the membrane by hot pressing[6,7] or most commonly onto the GDL, which is then hot pressed onto the membrane[8,9]. A number of methods have been developed for the application of the ink, including spraying[10], brushing[11], screen printing[12], tape casting[13] and rolling[14]. Glycerol is often added to adjust the viscosity of the ink. Pore forming materials, e.g. ammonium salts, and sparingly soluble fillers such as lithium carbonate are added to adjust the fine and coarse porosities respectively[15].

Conducting plates, usually graphite or stainless steel, are attached to each end of the cell to draw off current and to ensure an even distribution of reactant gas to all parts of the gas diffusion layer. For this purpose flow channels are etched into the inner surface of the plate in a variety of configurations. Initially, multichannel configurations were widely used, but the industry standard is now the serpentine geometry. More recently, Morgan Fuel Cell (UK) have pioneered a Biomimetic plate, which mimics the branching structure found in lungs and is 17% more efficient than the serpentine geometry. The additional functions of the current collector plate are to provide mechanical support for the MEA and to act as a heat sink, which is achieved by incorporating air or water-cooled channels into the plate. Air cooling is generally used for low power applications, with water cooling necessary for higher power applications.

The ideal properties for current collector plate materials are high electrical and thermal conductivity, high corrosion resistance, low contact resistance with the GDL and a similar thermal expansion coefficient to neighbouring components. Machined graphite was used in early technologies but its high cost has led to the increased use of the following materials:

1. Carbon-carbon composites – produced by injection moulding of carbon-graphite resin.
2. Carbon-polymer composites – produced by hot moulding of a carbon or graphite filler in a thermosetting or thermoplastic matrix (e.g. PVDF and carbon black).
3. Metals – pressed or cut metal sheet/foam made of stainless steel or coated titanium.

As fuel cell durability test times have increased, corrosion problems with both graphitic and metallic plates have emerged. As always, a compromise between performance and cost is necessary. Sealing is another important issue, as gas leakage between components can lead to performance loss. Silicone gaskets are commonly used and the selection of compression force has a marked effect on cell performance.

Since a single PEMFC produces a voltage of 0.6-0.7 V under typical load, many cells must be arranged in series to achieve high power outputs. Such a series of cells is known as a fuel cell stack. Here, each plate conducts current from the positive terminal of one cell to the negative terminal of the next and is therefore termed a bipolar plate. Engineering of fuel cell stacks is a highly complex and often convoluted process, which requires compressors, humidifiers, cooling systems, pumps, power conditioners and in some cases fuel reformers. The complexity of balance of plant engineering adds significant cost to fuel cell systems. Balance of plant malfunctions

currently account for a significant fraction of failures in service because of this complexity and the fact that many components have not been designed or optimised for fuel cell applications.

About 50% of maximum power is available on start up and full operating power is available after about three minutes under typical conditions. The low operating temperature (normally 70 – 85 °C) also means that thermal shielding is unnecessary. The excess heat may be used to heat water but is not sufficient to generate steam for fuel reforming. The connectivity of fuel cells to the electrical grid and in hybrid systems such as battery/fuel cell vehicles is of increasing interest to electrical engineers. The response time of fuel cells to changes in load have been demonstrated to be at least two orders of magnitude faster than that required for most applications[16]. Modelling of power management in such systems is developing in complexity but is outside the scope of this review.

In recent years attention has been increasingly focused on the durability of PEM fuel cells in service. The most common degradation modes of PEMFC stacks are membrane failure, sintering and corrosion of the electrocatalyst, poisoning, flooding of reaction sites, fuel crossover and corrosion of bipolar plates. Degradation is most severe when the MEA is highly stressed, e.g. by rapid fluctuations in load or by running at high current densities for extended periods, and when non-uniform distribution of reactants and/or temperature occurs. While membrane failure is the major lifetime constraint, the other degradation modes cause a gradual decrease in the output voltage of the stack. The 2002 DTI Sustainable Energy Route Map for fuel cells sets a performance degradation target of <1% over 1000 hours operation. In the long term, fuel cell stacks for stationary applications need to reach 40,000 h operation, while those for more demanding automotive applications will require 4000 h, without unacceptable loss of performance. This review summarises current understanding of performance degradation in such devices, including an assessment of experimental techniques employed to characterise fuel cell performance and durability and a discussion of the various degradation modes.

2. EXPERIMENTAL TECHNIQUES

A wide range of experimental techniques is available for the characterisation of fuel cell performance. Electrochemical techniques are used in combination with structural and chemical analysis to correlate the performance of the cell with the material properties of the various components. Durability tests are the only reliable indicator of long term performance but such tests are time consuming as they can last for thousands of hours. The development of reliable accelerated ageing tests has yet to occur but will follow from better understanding of degradation mechanisms. In this section the various experimental techniques employed in the characterisation of fuel cell performance are summarised under four headings:

1. Electrochemical techniques
2. Structural characterisation
3. Chemical analysis
4. Modelling

The strengths and weaknesses of each technique are assessed and selected data from the literature are presented to illustrate the type of information obtained by each method.

2.1 ELECTROCHEMICAL TECHNIQUES

In-situ voltammetry

The standard electrochemical technique for characterising the performance of both single cells and stacks is the measurement of potential as a function of current density under a set of constant operating conditions. The effect of composition, flow rate, temperature and relative humidity of the reactant gases may be varied systematically to investigate their effect on cell performance. An electronic load is used to dissipate the power generated in these experiments while maintaining the accuracy of the measurements. A plot of potential against current density is known as a polarisation curve and yields information about the losses in the cell or stack under service conditions. A typical polarisation curve for a single hydrogen/air fuel cell is shown in Fig. 2. At low current densities the majority of the losses are due to kinetic limitations at the electrocatalyst surface. Since the exchange current density for hydrogen oxidation on Pt is three orders of magnitude higher than that for oxygen reduction on Pt, the activation losses at the cathode dominate the cell behaviour at low current densities. As the current density increases, the IR drop across each component of the fuel cell increases and ohmic losses become significant. This is evident in the linear portion of the polarisation curve at intermediate current densities. At high current densities, mass transport effects dominate and the cell performance drops drastically. Transport of reactant gas through the pore structure of the backing layers and electrocatalyst layers is the limiting factor here.

Polarisation curves provide information about the performance of the cell or stack as a whole. While they are a useful indicator of overall performance under service relevant

conditions, they do not yield much information about the performance of individual components and are incapable of resolving time dependent processes occurring in the fuel cell. For this latter purpose current interrupt methods or impedance measurements are more commonly used. Polarisation curves are often converted to plots of power per unit area versus current density by multiplying the potential by the current density at each point on the curve.

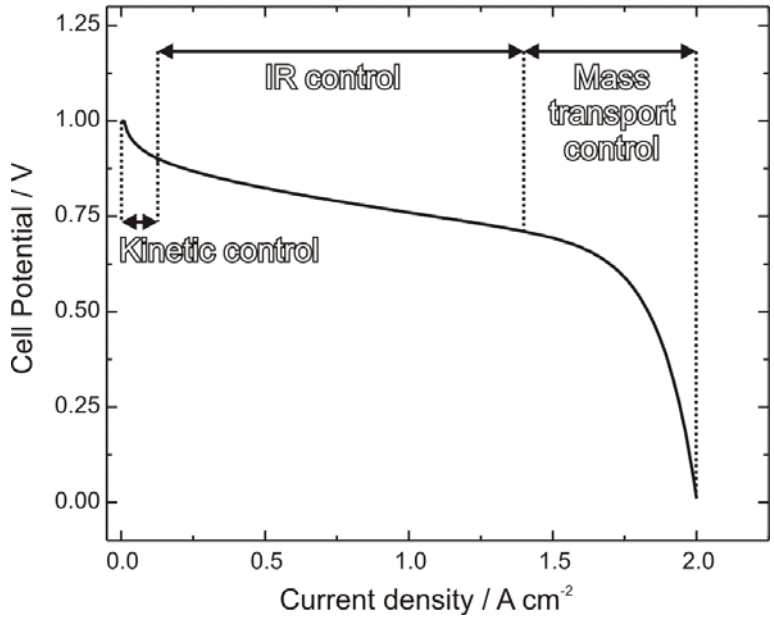

Fig. 2: Typical polarisation curve for a PEMFC.

In studies of PEMFC cathodes it is important to keep the anode composition and loading constant if it is to be used as a reference electrode. The reversibility of the HOR on Pt is considered sufficient for this purpose, although when reformate is fed to the anode, the polarisation of both electrodes may be comparable. Voltammograms may be corrected for the IR drop across the membrane by measuring its high frequency resistance using current interrupt or impedance methods.

The performance of MEAs fabricated using a range of different techniques has been well characterised by polarisation measurements in the literature. Performance is usually expressed in terms of output current density at a fixed potential, typically 0.6 V. A typical well performing single PEMFC yields a current density in the range 0.1-5 A/cm^2 at 0.6 V. The performance depends primarily on the activity of the electrocatalyst layer, the quality of material components and the flow rate and purity of the reactant gases. The best performance is obtained when pure oxygen is fed to the cathode, but in most practical systems air is used. The nitrogen in air acts as a diluent and as a result the performance of H_2/air fuel cells suffers from both open circuit losses and mass transport limitations relative to H_2/O_2 fuel cells. By pressurising the air on the cathode side, substantial gains in performance may be obtained. However

the energy cost of compressing the gas means that there is an optimum pressure beyond which it is not economically feasible to increase the performance any further.

In air-breathing PEM fuel cells, free convection of oxygen is the dominant mass transfer process at the cathode. Here transport of oxygen is controlled by the density difference between oxygen-depleted air at the cathode surface and air at the inlet. Li et al showed by comparison of polarisation curves obtained in free convection mode with those obtained under forced convection of air showed that cell performance was unaffected below a certain threshold current density governed by the rate of mass transport under free convection[17]. With their particular cell, a current density of 200 mA/cm^2 was achievable in free convection mode; above this value the current density dropped drastically. An upward orientation of the cathode surface was found to maximise cell performance.

A survey of the literature reveals that MEAs produced by more recent fabrication techniques have shown a reduced output current density. This is due to the requirement to reduce manufacturing costs, since a compromise between cost and performance is required for commercialisation of the technology. The current drive is to reduce platinum loadings and to develop cheap fabrication processes which will be commercially viable when scaled up to mass production. Initially electrocatalyst layers consisted of unsupported platinum black with a loading of at least 4 mg/cm^2. The use of nanoparticles supported on high surface area carbon and the increase of catalyst utilisation by the incorporation of ionomer into the active layer has reduced the Pt loading to < 0.1 mg/cm^2. Further decreases should be possible with improvements in the understanding of charge and mass transport in the active layer.

Below around 50 cm^2, the active area of the cell is too small to accurately simulate the flow field patterns required in large stacks. Low gas flow rates at low current densities are also difficult to control. However, the use of large active areas is not straightforward on a laboratory scale due to the difficulty and cost of fabrication and the greater magnitude of the total current. Large currents not only require larger and more expensive load banks, but also pose problems for techniques such as impedance spectroscopy, where the bandwidth may be restricted under high load.

During fuel cell operation, usually only integral values such as current, voltage and impedance are measured, which do not give any information about the spatial distribution of reactants and electrochemical activity over the surface. Segmented electrodes have been increasingly used to investigate the distribution of current density over the active area of the cell. Each segment of the electrode is isolated from the others by an insulating material and the contribution of each segment is monitored in real time. The anode is usually segmented as its performance is less disturbed than that of the cathode. Adcock et al used a circular active area with a segmented current collector plate arranged in pie-shaped sections[18]. Cleghorn et al[19] used a printed circuit board technique to segment the current collector in order to investigate the effect of air flow rate. At high flow rates, the performance increased from inlet to outlet due to a lowering of membrane resistance, while at flow rates less than three

times stoichiometry, the performance dropped from inlet to outlet due to oxygen depletion along the channel. Noponen et al[20] used a segmented anode consisting of 4 rows and 8 columns to examine the effect of O_2 and humidity levels on the current distribution in a PEMFC. The current distribution in conditions of high humidity and with O_2 as the oxidant is compared with that under conditions of low humidity with air as the oxidant in Fig. 3. In the latter case, a substantial decrease in performance is correlated with a very uneven distribution of current across the active area.

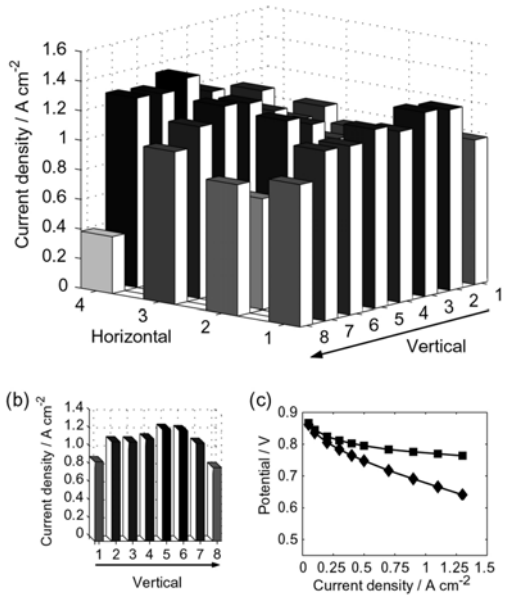

(i)

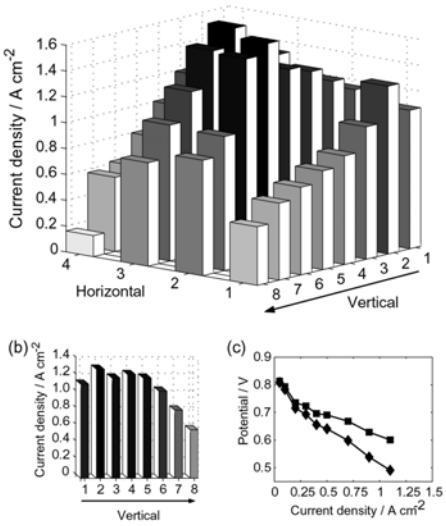

(ii)

Fig. 3: Comparison of current density distribution in a segmented anode PEMFC under (i) high humidity in O_2 and (ii) low humidity in air[21].

Variants on this technique have been developed using shunt resistors embedded in the current collector plate[22] and in-situ IR spectroscopy to study water transport[23]. Segmented electrode studies are particularly useful to aid design of flow fields and water management strategies. Other techniques to measure two-dimensional current distribution in PEM fuel cells include sensing of stray magnetic field due to local currents with Hall probes[24,25] or SQUIDs[26].

Ex-situ voltammetry

The electrochemical performance of a single electrode may be examined ex-situ by cyclic voltammetry (CV) and other common electrochemical techniques. Such half-cell experiments are carried out in a standard three electrode cell with an aqueous solution of acid (typically 0.5 M H_2SO_4) used to simulate the proton-conducting electrolyte in a PEMFC. Half cell experiments are a convenient and relatively fast method of screening electrocatalysts and comparing different MEA preparation techniques.

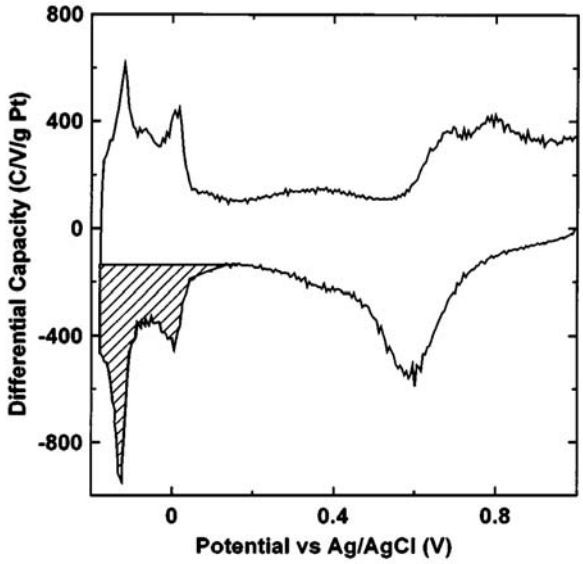

Fig. 4: Illustration of the method used to calculate active surface area using hydrogen adsorption voltammetry[27]. The shaded area represents the charge due to hydrogen adsorption.

When the half cell experiment is carried out in solution purged with an inert gas such as nitrogen, integration of the hydrogen adsorption peak may be used to measure the active surface area of the electrocatalyst. An example of such a voltammogram for a Pt electrocatalyst is shown in Fig. 4. The shaded area represents the total charge arising from hydrogen adsorption. The baseline is the capacitative current due to charging of the electrode double layer. This total charge may be converted to an active surface area (cm^2/g) using a proportionality constant, e.g. 210 $\mu C/cm^2$ for a

platinum surface[28]. The Brunauer-Emmett-Teller (BET) method is used to calculate the effective surface area from nitrogen adsorption isotherms and is often quoted by manufacturers of electrocatalysts. Ratios of active surface area to geometric surface area of order 10^3 are commonly obtained for PEMFC electrocatalysts. Carbon monoxide stripping voltammetry is another common technique for determining the active surface area, operating under the same principle.

Many half-cell studies have focused on the oxygen reduction reaction (ORR) since it has a significantly larger overpotential on Pt than the hydrogen oxidation reaction (HOR). Kinetic parameters such as exchange current density and Tafel slope may be readily extracted from voltammograms obtained in O_2-saturated solution.

Cyclic voltammetry is the most common ex-situ diagnostic tool for probing the electrochemical activity of electrocatalyst layers. Most PEMFC electrocatalyst layers consist of a mixture of carbon-supported Pt and Nafion or Nafion-like ionomer. Most studies are divided between the determination of active area of the electrocatalyst[29] and the elucidation of the kinetics of the ORR at the triple phase boundary (TPB) between ionomer, catalyst and open pore[30]. The undesirable effects of poisons such as CO, which adsorb onto the electrocatalyst surface thereby decreasing the number of available catalytic sites, have been well documented[31].

Stevens and Dahn compared the active surface area of a high surface area Pt/C electrocatalyst (E-Tek BP2000, BET surface area 1300 m^2/g) to that of a lower surface area Pt/C electrocatalyst (E-Tek XC72, BET surface area 270 m^2/g) as a function of Pt loading and particle size. The electrocatalysts were mixed with 5% Nafion in a mixture of aliphatic alcohols, water and isopropanol and deposited on a glassy carbon electrode. Voltammograms were obtained in a three electrode cell containing 0.1 M HCO_4. An optimum Pt particle size of 2 nm was identified for both types of electrocatalyst[32]. The XC72 samples showed a marked decrease in active surface area with increasing Pt loading, while no distinct trend was observed for the BP2000 samples.

Gloaguen et al used a rotating disk electrode (RDE) to allow correction of mass transport effects in solution[33]. The active layer consisted of 5% Nafion with 30 wt% Pt/Vulcan XC72 (E-Tek) and the electrolyte used for the CV experiments was 0.5 M H_2SO_4. Tafel plots for the ORR showed a double Tafel slope, with the slope at high potentials relevant to PEMFC operation close to 2.3RT/F. An exchange current density of 7×10^{-11} A/cm^2 was obtained at 20 °C, 1 atm above 0.8 V, which compares well with that obtained for bulk platinum in various electrolytes. An optimum Pt particle size of 3.5 nm was identified in this study.

The kinetics of the ORR are governed by the amount of triple phase boundary in the active layer of the cathode. Due to the complexity of the heterogeneous structure of the active layer, the amount of TPB is difficult to determine. More detailed characterisation of the TPB in PEMFC active layers is required to understand the correlation between electrocatalyst microstructure and performance. Pt microelectrodes have been used to study the ORR at solid state Pt/Nafion

interfaces[34,35]. Recently O'Hayre and Prinz patterned circular Pt-electrocatalyst microstructures on Nafion using a focused ion beam (FIB) system and investigated the ORR kinetics using impedance spectroscopy[36]. For electrodes smaller than 40 μm a direct relationship between electrode circumference and faradaic impedance was observed, indicating that the ORR kinetics scale with length of TPB. The authors proposed the use of a TPB width term in a coupled reaction/diffusion model to bridge the results of area-related and perimeter-related ORR kinetics.

Ex-situ voltammetry may also be used to investigate the corrosion susceptibility of candidate bipolar plate materials in simulated PEMFC environments. Borup and Vanderborgh calculated a maximum tolerable corrosion current of 1 mA/cm^2 assuming that most of the corrosion product passes out of the fuel cell in the exhaust water[37]. They obtained polarisation curves for aluminium, carbon-coated aluminium and titanium alloy plate materials in both oxidising and reducing environments to simulate cathode and anode conditions respectively. Only the titanium alloy material satisfied the corrosion constraints under both sets of conditions. Li et al[38] examined the corrosion behaviour of TiN-coated AISI 316 stainless steel in a simulated PEMFC environment consisting of 0.01 M HCl/0.01 M Na_2SO_4 solution (pH 4) bubbled with pure oxygen or hydrogen. The stainless steel substrate was in the active state in the anode environment and in the passive state in the cathode environment. The TiN-coating displayed better corrosion resistance and passivity under both sets of conditions.

Current interrupt method

The ohmic losses in a fuel cell may be isolated by the current interrupt method. The principle behind this technique is that the ohmic losses vanish much faster than the electrochemical overpotentials when the current is interrupted[39]. The fuel cell is operated at a constant current before the measurement and a voltage transient is recorded upon interruption of the current, as shown schematically in Fig. 5. The ohmic losses disappear almost immediately and the electrochemical overpotentials decay to the open circuit value over a longer timescale. It is therefore important that the data acquisition for the voltage transient is as rapid as possible in order to adequately separate the ohmic and activation losses

Buchi et al determined the time resolution required by considering the relaxation processes in the membrane[40]. They estimated the dielectric relaxation time, τ, for the membrane using the equation:

$$\tau = \rho\varepsilon_r\varepsilon_0 \qquad (3)$$

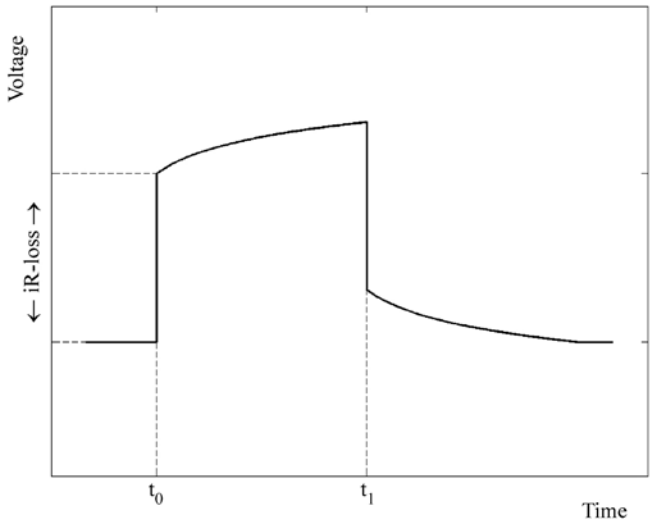

Fig. 5: Ideal voltage transient in a PEMFC after current interruption[41].

where ρ is the membrane resistivity, ε_r is the relative permittivity and ε_0 the permittivity of free space. Conservatively taking ρ = 20 Ωcm and ε_r = 79 (the low frequency value for water) yielded $\tau = 1.4 \times 10^{-10}$ s. Since the dielectric relaxation process will decay to below 1% of its original value after 4.6τ, the ohmic losses should disappear on a timescale of half a nanosecond in the worst case. Since there is little theory available on the fastest electrochemical relaxation processes in PEM fuel cells, the authors assumed a conservative limit of 10^{-8} s, based on observations of water electrolysis membranes[42]. They concluded that the time window for accurate current interrupt measurements on the membrane is between 0.5 ns and 10 ns.

Mennola et al showed that the current interrupt technique could be used to isolate poorly performing individual cells in a stack[43]. An example of a voltage transient for an individual cell is shown in Fig. 6. At high air flow rates, cells in the middle of the stack showed up to 21% higher ohmic losses than average, which was attributed to dehydration of the membrane. Their results showed good agreement between the ohmic losses in the entire stack and the sum of the ohmic losses in each individual cell.

Jaouen et al recently extended the use of this technique to the study of electrode processes in PEM fuel cells[44]. They found that analysis of the voltage relaxation curve after the disappearance of the ohmic losses could yield information on the electrochemical performance of the electrodes. An example of relaxation curves at a number of different current densities is shown in Fig. 7. The plateau at short times is indicative of O_2 diffusion limitation, while limitation by proton migration results in no plateau at short times and a transition to a Tafel slope at longer times. A model containing expressions for Tafel kinetics, oxygen diffusion in agglomerates, proton migration and double layer capacitance was developed[45], which fitted the experimental data well up to a current density of 200 mA/cm^2.

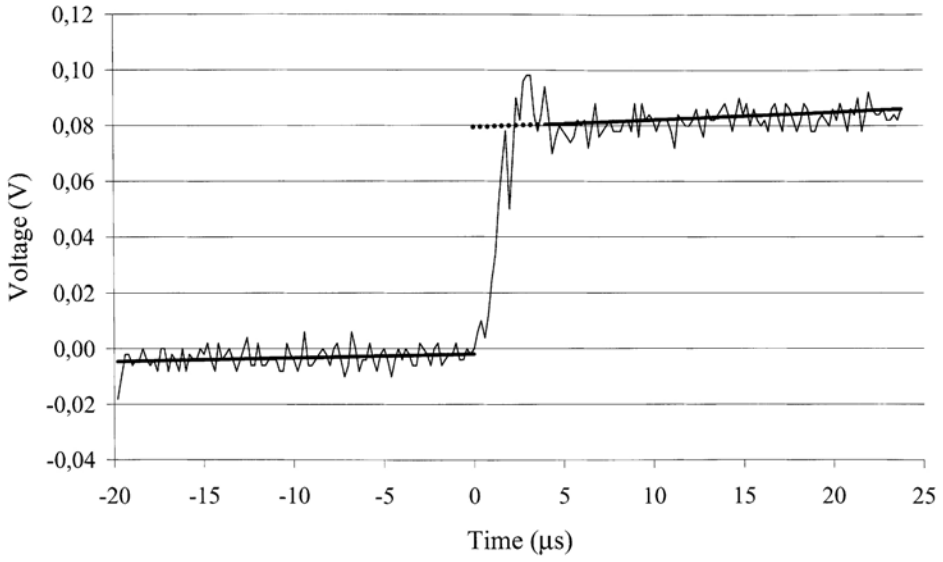

Fig. 6: Voltage transient for an individual cell in a PEMFC stack during current interruption[46]. Extrapolation is indicated by the dotted line. Current density before interruption is 400 mA/cm^2.

The effect of cathode gas humidifier temperature, T_{ca}, on the MEA resistance was investigated by Abe et al using the current interrupt technique[47]. They found that the MEA resistance increased by 3.5 mΩ when T_{ca} was lowered from 80 °C to 35 °C. Electrochemical measurements showed that this increase in resistance was divided between the membrane (1.1 mΩ), charge transfer resistance (1.2 mΩ) and an unknown resistance (1.2 mΩ).

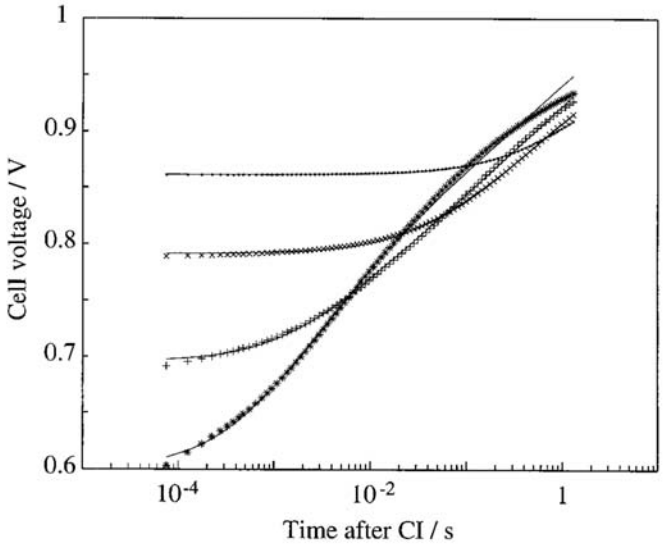

Fig. 7: Relaxation curves of PEMFC voltage after current interruption for current densities of (.) 1, (x) 10, (+) 100 and (*) 400 mA/cm^2 before interruption[48].

Impedance spectroscopy

Impedance spectroscopy is a powerful tool for the analysis of electrochemical systems. In contrast to linear sweep and potential step methods, where the system is perturbed far from equilibrium, a small ac voltage perturbation is applied to the cell and the amplitude and phase of the resulting signal are measured as a function of frequency. This allows the resolution of dynamic processes occurring on different timescales in the system being studied.

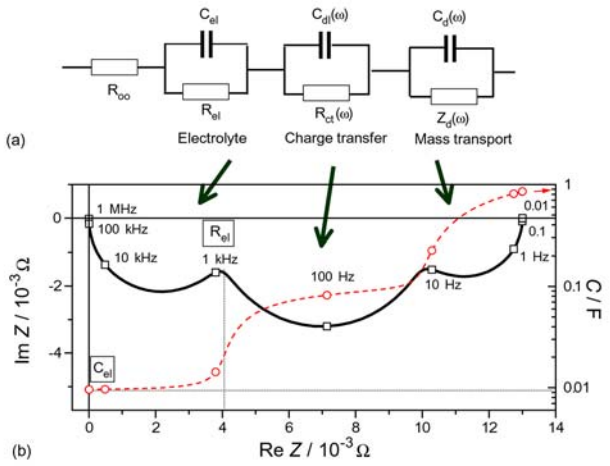

Fig. 8: (a) General equivalent circuit for a PEMFC (b) Schematic frequency response of impedance and capacitance[49].

Impedance spectra are conventionally plotted in both Bode and Nyquist form. In a Bode plot, the amplitude and phase of the impedance is plotted as a function of frequency, while in a Nyquist plot the imaginary part of the impedance is plotted against the real part at each frequency. A typical Nyquist plot for a PEMFC consists of three depressed semicircles as shown in Fig. 8, where the frequency increases from right to left. The major axis of the high frequency arc is proportional to total ohmic resistance of the cell, which can be directly compared to that obtained from current interrupt measurements. The major axis of the second arc is a measure of the charge transfer resistance of the electrochemical reaction, which is usually dominated by the impedance of the cathodic reaction. The low frequency arc reflects the impedance due to mass transport limitations, which is usually absent for systems fed with oxygen.

The measurement of the magnitude and phase of the impedance as a function of frequency may be readily analysed in terms of equivalent circuits. In this type of analysis, the cell response is modelled on that of an electrical circuit containing combinations of resistors and capacitors, each representing a particular physical or chemical process. In general, a resistor represents a conductive path, such as ion migration in electrolyte or the charge transfer accompanying an electrode reaction. A capacitor represents a space charge layer, such as the electrical double layer at the

electrode/electrolyte interface. Mass transport phenomena, such as diffusion to an electrode surface, are represented by a Warburg impedance, which is manifested in a straight line with a slope of unity in the Nyquist plot at low frequencies. A constant phase element (CPE), a non-intuitive circuit element that has no analogue in conventional electronics, was invented to describe the behaviour of non-ideal surfaces. The phase of the CPE is independent of frequency and represents a distribution of time constants due to the inhomogeneity of the surface. The CPE may be represented by a network of RC-circuits with time constants spanning orders of magnitude and may be modelled by fractal geometry.

A high power potentiostat, for which the current limit is typically 50 A, is required for full range impedance measurements on PEM fuel cells. Measurements on large area cells or stacks may therefore only be carried out at low currents. The use of long leads should be avoided as this results in inductive effects at higher frequencies. For this reason, twisted pairs should be used where possible.

Springer et al[50] showed that simultaneous fitting of impedance spectra obtained at different potentials could be used to evaluate sources of PEMFC losses. They found that insufficient cell humidification led to simultaneous decreases in electrocatalyst activity, membrane conductivity and active layer conductivity. Lefebvre et al reported that the impedance response becomes dominated by charging of the cathode catalyst double layer through the ionic resistance when the cathode is purged with nitrogen[51]. Fitting of experimental data generated a conductivity profile of the catalyst layer, which yields information on the ionomer distribution close to the membrane.

The issue of the changing state of the system with time was addressed by Schiller et al[52]. Since the recording of an impedance spectra takes a finite time, with the recording time increasing with decreasing frequency, the system is in a different state at the end of the measurement than it was at the beginning. To eliminate the effects of drift, a series of impedance measurements are carried out at distinct time intervals and the elapsed time is included as a third axis in the experimental plot. An appropriate smoothing function may then be used to interpolate the impedance values. The authors used this technique to assess the effects of hindered water removal on PEMFC performance. The low frequency impedance increased from 50 mΩ to 1 Ω after 8 hours, which was related to an equivalent circuit containing RC circuits for both cathode and anode in series with a membrane resistance and a wiring inductance.

Several authors have used impedance techniques to study CO poisoning of the anode. Ciureanu and Wang[53] observed pseudo-inductive behaviour above 0.3 V, which they attributed to a rate determining step of oxidation of adsorbed CO by adsorbed Pt-H_2O. One issue with impedance measurements on fuel cells is the separation of the impedances of anode and cathode. Wagner and Gulzow[54] demonstrated that by carrying out the measurements in galvanostatic rather than potentiostatic mode the change in cell impedance is mainly due to that of the anode. The anodic charge transfer resistance increased from 3 mΩ to 500 mΩ after around 4 hours exposure to 100 ppm CO.

Interpretation of impedance spectra is still an open question in the literature. Andreaus et al proposed that the low frequency impedance commonly ascribed to diffusion

limitation in the cathode active layer may equally be due to dehydration of the membrane close to the anode at high current densities[55]. They demonstrated that this effect was more pronounced with thicker membranes, where back-diffusion of water from the cathode is less efficient, resulting in an increased membrane resistance and an increased activation overpotential as catalyst sites become inactive due to the low proton mobility in the dehydrated region. Romero-Castanon et al identified a faradaic contribution to the impedance in the low frequency range[56], both in the presence and absence of faradaic currents at high frequencies.

Four point probe techniques

It is very difficult to resolve the resistances of individual components in a fuel cell using two point probe techniques such as current interrupt and impedance spectroscopy. The van der Pauw (VDP) method is a four point probe technique that can be used to measure both local and large scale conductivity depending on the location and separation of the probes. The conductivity is determined by measuring the resistance of the sample in two directions and substituting the values into an empirical formula[57]. This technique has been applied to PEM fuel cells[58], although it should be noted that only the lateral conductivity is measured, rather than the through thickness conductivity which is more relevant to fuel cell applications. However, the VDP technique can still yield valuable information on crack formation and membrane deterioration.

2.2 STRUCTURAL CHARACTERISATION

Imaging techniques

The most common imaging techniques used in the analysis of fuel cell materials and components are scanning electron microscopy (SEM), which is used for characterisation on a micron scale, and transmission electron microscopy (TEM), which is used for nanoscale characterisation. SEM is well suited to the examination of pore structure in the GDL and to the measurement of membrane and electrode thickness in cross-section[59]. An example of a SEM image of a MEA cross-section is shown in Fig. 9. The preparation of the MEA cross-section is usually carried out by cooling the sample in liquid nitrogen before fracture to avoid deformation[2]. Although time consuming, this technique is preferable to measuring the thickness directly with a micrometer. This is due to the large uncertainty in electrode thickness when compared to that of the membrane and the fact that only the total thickness can be measured for a real MEA[60].

TEM is used to characterise the particle size and distribution of the electrocatalyst and support. A typical electrocatalyst consists of platinum particles of 2-3 nm in diameter, supported on agglomerates of carbon particles of ~ 30 nm in size, as shown in the TEM micrograph in Fig. 10. Both of these imaging techniques and their variants (HR-SEM and STEM) are therefore extremely useful in the systematic investigation of the correlation between material fabrication methods and cell performance. Atomic

resolution scanning probe techniques such as atomic force microscopy (AFM) and scanning tunnelling microscopy (STM) are not generally applicable to fuel cell materials due to their inhomogeneity and high surface roughness.

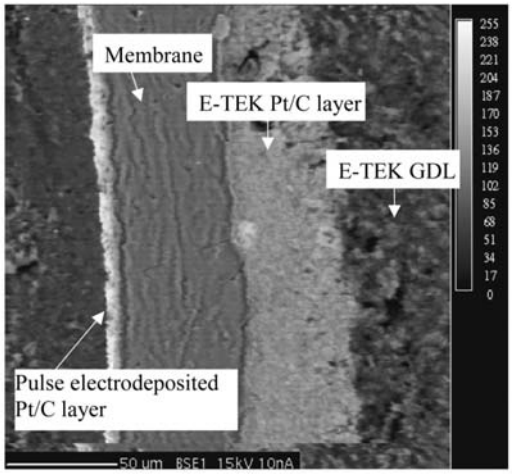

Fig. 9: Backscattered electron image of a typical MEA cross-section[61].

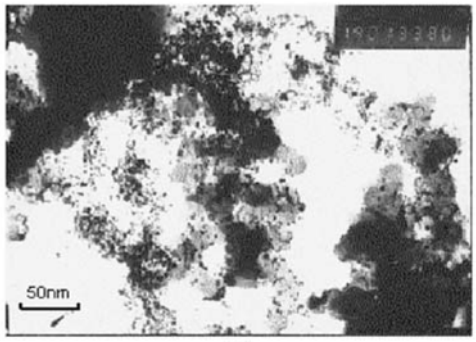

(c)

Fig. 10: TEM micrograph of Pt/C electrocatalyst[62].

X-ray diffraction (XRD)

Characterisation of crystalline materials may be carried out by X-ray diffraction (XRD), which provides a direct probe of the size and structure of the crystal lattice. XRD is most commonly used for the characterisation of the electrocatalyst and membrane structure in PEM fuel cells. Diffraction of electromagnetic radiation occurs when the wavelength of the incident radiation is comparable to the interatomic spacing. This condition is satisfied by X-rays, whose wavelength is of order 0.1 nm. X-rays are specularly reflected from successive parallel planes of atoms in the crystal, with each plane reflecting only a tiny fraction of the incident radiation. Diffraction peaks may be detected at certain angles where the reflected beams interfere constructively. The position and intensity of these peaks are unique to each crystalline material, which allows for relatively straightforward identification. The sharpness of

the peaks is an indication of the degree of crystallinity, which is an important parameter for PEMFC membranes.

Porosimetry

From a mass transport perspective, the porosities of the active layer and GDL are of critical importance to the operation of the fuel cell. If the thickness and composition of the active layer are known, the porosity can be calculated simply by dividing the volume of the solid phase by the total volume of the electrode. Otherwise, the porosity can be determined by filling the pore structure with an inert solvent such as toluene[63]. Mercury or gas porosimetry are often used to characterise the pore size distribution of both the active layer and GDL. Mercury porosimetry is used to characterise larger pore sizes (3 nm – 300 μm), while nitrogen porosimetry is suited to smaller pore sizes in the range 0.5 nm – 100 nm. Relatively large volumes of sample are required, which often means that the sample has to be cut into small pieces and stacked in the sample holder. This perturbs the pore size distribution above 1 μm, making the quantitative determination of porosity more difficult. For low pore sizes, the high pressure required may result in collapse of the pore structure[64].

Several groups have attempted to characterise the microstructure of the active layer using mercury and gas porosimetry. Watanabe et al characterised the pore structure of active layers consisting of a mixture of ionomer and carbon-supported platinum and found that there were two distinctive pore distributions with a boundary at around 0.1 μm[65]. The primary (smaller) pore size was identified with the space between the particles in the agglomerate of the carbon support while the secondary pore size was identified with the space between the agglomerates. Uchida et al later postulated that the ionomer and therefore the reaction sites were confined to the secondary pores[66]. They examined the performance of single cells as a function of ionomer content in the active layer. The volume of the secondary pores (0.04 – 1 μm) decreased linearly with increasing ionomer content, while that of the primary pores (0.02 – 0.04 μm) remained unchanged, confirming that the ionomer was only present in the larger pores[67]. The primary pores therefore act as gas channels.

More recently Lundblad showed that different fabrication procedures result in very different microstructures in the active layer. He found that the distribution of ionomer in the active layer was critically dependent on the mixing treatment of the catalyst ink. Solvents in which the ionomer is more soluble, such as ethanol or isopropanol, increase the wetability to carbon by decreasing the surface tension. In this work, the electrocatalyst powder was mixed, using ultrasound, with a 5% Nafion solution in propanol, methanol and water, containing proprietary dispersant additives from DuPont Fluoroproducts Ltd. A more uniform distribution of ionomer was observed, even penetrating and/or encapsulating the small primary particles (30 nm) of the carbon support[68]. Lundblad pointed out that the use of butyl acetate, in which the ionomer is less soluble, would explain the different ionomer distribution in the work of Uchida et al. Different pore structures require different electrochemical models in order to understand their performance.

Gamburzev and Appleby investigated the effect of incorporating proprietary pore forming additives to the cathode electrocatalyst-ionomer ink. An optimal amount of pore former (33 wt%) was identified for the MEAs studied, which yielded a performance of 340 mA/cm^2 on air at 0.7 V compared to 210 mA/cm^2 with no pore former[69].

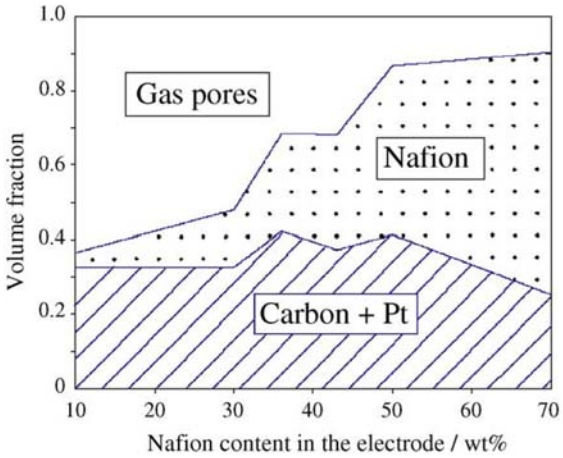

Fig. 11: Volume fraction of gas pores, Nafion and Pt/C in an electrode as a function of Nafion content[70].

The influence of Nafion content on the structure and performance of the cathode active layer was investigated by Gode et al[71]. The volume fraction of Nafion, Pt/C and open pores as a function of Nafion content is shown in Fig. 11. The porosity does not vary much between 10 wt% and 30 wt% Nafion, but decreases dramatically at higher Nafion contents. Data obtained from impedance spectroscopy were analysed using an agglomerate model[72] developed by the authors, which showed that the model broke down above 45 wt% Nafion. This was interpreted as a blocking of the pores and a non-percolating Nafion system at high Nafion contents.

The influence of porosity of the gas diffusion layer on PEMFC performance has been investigated by a number of authors. The GDL usually consists of a thin layer of carbon black mixed with PTFE, coated on a sheet of macroporous carbon cloth. The PTFE is incorporated into the GDL to facilitate water removal from the electrode and prevent flooding. Although the GDL is often considered a minor component of the fuel cell, it has been demonstrated that its composition can have a substantial effect on overall cell performance. If the GDL is too thick, ohmic and mass transfer losses will be too high, while if it is too thin the mechanical strength and contact resistance may be poor. Most of the effects of GDL properties on fuel cell performance are observed at high current densities, where mass transport is the rate limiting factor. Prasanna et al[73] recently carried out a study of the effect of different commercial GDL materials on the performance of single PEM fuel cells and concluded that gas permeability and pore diameter were the most important physical properties. They found that a mean pore size of above 60 μm results in greater losses at high current densities due to water droplet formation at the interface of the GDL and the active layer. The gas

permeability was severely affected by the hydrophobicity of the GDL, which varies with PTFE content. The authors identified an optimum PTFE content of 20%. The influence of the porosity of the GDL on cell performance was investigated by Chu et al using numerical simulation[74]. The results showed that a higher average porosity leads to a lower mass fraction of oxygen in the GDL due to higher consumption of oxygen in the catalyst layer, meaning that a fuel cell with a higher surface overpotential will require a GDL with a higher porosity. However, the simulations did not take into account flooding of the pores, which would limit the porosity level in practice.

2.3 CHEMICAL ANALYSIS

A variety of spectroscopic techniques have been used to characterise the composition and chemical state of fuel cell materials. These techniques are particularly useful for the detection of chemical degradation in fuel cell components in long term tests. Most of the studies in the literature are concerned with the chemical properties of the active layers and the membrane.

X-ray photoelectron spectroscopy (XPS)

X-ray photoelectron spectroscopy (XPS) yields quantitative information on the surface concentrations of elements and their binding states. The energy of photoelectrons ejected from the sample by an incident X-ray beam is measured, allowing identification of each element from its characteristic energy signature. A compositional map of the surface is obtained from analysis of the area under each peak. The XPS technique is highly surface specific due to the short range of the photoelectrons that are excited from the solid. Depth profiles of up to 100 nm may be obtained by alternately recording XPS spectra and removing surface layers by ion etching.

Energy dispersive X-ray spectroscopy (EDX)

Energy dispersive X-ray spectroscopy (EDX or EDS) operates in the opposite mode to XPS, i.e. the energy of X-rays emitted when an electron beam impinges on the surface is measured. Most EDX systems are built into SEM or TEM units to enable in-situ analysis of surface composition in combination with images of the surface. Again, each element has a characteristic X-ray peak, the integral of which is proportional to its composition. Element mapping is a common technique whereby the X-ray energy is fixed to detect a particular element and the beam is rastered over the surface to obtain a spatial distribution map for that element. One issue with the analysis of MEAs is the distinction between Nafion and PTFE in the active layer. Since Nafion is a derivative of PTFE, the sulphur peak could in principle be used to distinguish the Nafion from the PTFE. However, the sulphur peak happens to coincide with that of platinum, which means that in practice the Nafion must be marked by ion exchange with alkali ions such as sodium[75].

X-ray absorption spectroscopy (XAS)

X-ray absorption spectroscopy (XAS) is a powerful technique that can yield information on the electronic structure and coordination of selected atoms. An X-ray beam is incident on the sample and the energy of the transmitted beam is measured as a function of the energy of the incident beam. A typical XAS spectrum is divided into two parts. The X-ray absorption near edge structure (XANES) provides information on the electronic structure of the material, such as density of states and orbital symmetries, while the extended X-ray absorption fine structure (EXAFS) reflects the coordination of the atom. The spectrum can be tuned to examine a particular type of atom in the system, e.g. a catalytically active site.

Rutherford Backscattering Spectroscopy (RBS)

Rutherford backscattering spectroscopy (RBS) involves measuring the number and energy of α-particles in a beam which backscatter after colliding with atoms in the near-surface region of a sample. With this information, it is possible to determine atomic mass and elemental concentrations versus depth below the surface. It is suitable for profiling the concentration of heavy elements such as platinum distributed in a matrix of lighter elements, which makes it ideal for the study of electrocatalyst layers in PEM fuel cells. The scattering cross section is proportional to Z^2, where Z is the atomic number, meaning that the platinum scattering is enhanced relative to that of the carbon support.

Secondary ion mass spectrometry (SIMS)

Secondary ion mass spectrometry (SIMS) is a technique whereby the surface of the sample is bombarded by a primary ion beam and the secondary ions emitted from the surface are detected by a mass spectrometer. When the mass spectrometer is set up to detect a certain element, a depth profile may be obtained as the sputtering time increases. SIMS is the most sensitive surface analytical technique due to the inherent sensitivity of mass spectrometric-based techniques.

Various other spectroscopic techniques such as infrared (IR) spectroscopy, Raman spectroscopy and electron paramagnetic resonance (EPR) have been used to a lesser degree by fuel cell research groups.

2.4 MODELLING

A great deal of work has gone into the development of mathematical models to simulate the performance of PEM fuel cells. In the majority of cases, the aim of the model is to reproduce experimental polarisation curves under various operating conditions. The models in the literature may generally be categorised as either empirical or steady state in nature. The empirical approach makes use of linear regression to produce best fits to experimental data in order to determine functional relationships between current density and fuel cell voltage. A more rigorous approach is the construction of a physical model of the fuel cell, using a set of equations which can be solved under steady state conditions. The complexity and sophistication of

such models has grown in tandem with understanding of transport properties in the membrane and active layers. For H_2/air fuel cells, the cathode performance dominates the cell behaviour under most conditions, so most effort has been concentrated on the cathode.

Empirical models

Kim et al[76] presented the following empirical equation, which produced a good fit to experimental data at several temperatures, pressures and oxygen compositions in the cathode gas stream.

$$E = E_0 - b \log i - iR - m \exp (ni) \quad (4)$$

The first term is the open circuit potential, the second represents the activation losses (in Tafel form), the third term covers the ohmic losses and the exponential term compensates for the mass transport losses. In this region the parameter n has a more pronounced effect than the parameter m. Amphlett et al[77] developed a similar model for a Ballard Mark IV single cell, which expresses relationships between current, voltage, pressure and temperature based on intuitive mechanistic principles. A semi-empirical model was later developed by Pisani et al, where the only empirical parameter is the ohmic overpotential and all other terms are derived from phenomenological mass transport and conservation equations[78]. This approach enabled an assessment of the effects of cathode flooding and local decrease in oxygen concentration. Lee et al[79] recently used artificial neural networks to fit experimental data obtained in a 300 cm^2 single cell, with a view to optimising cell, stack and system design. Such empirical models are useful in establishing parametric relationships but provide little insight into the operation of the fuel cell on a more fundamental level.

Steady state models

A wide range of steady state models, of varying complexity and dimensionality, have been developed to simulate PEMFC performance over the past decade. These include 1D models, where the spatial dimension is parallel to the flow of current, 2D models, where the planes considered are perpendicular to the cell plates, and more recently complex 3D models.

Springer et al[80] presented a 1D model for a well-humidified PEMFC, which considered losses from kinetics, transport in the active layer and gas transport in the cathode GDL. They found that the overall losses in well-humidified H_2/O_2 cells could be well described by the sum of the high frequency (membrane and contact resistance) and cathode activation losses. Bernardi and Verbrugge[81] developed a similar model using the Nernst Planck equation, Schlogl's velocity equation, the Butler-Volmer equation and the Stefan-Maxwell equation. The results of a typical model calculation of the contributions to fuel cell losses for the base case (no mass transport limitation) are shown in Fig. 12. The cathode activation overpotential is

clearly the dominant source of loss, although ohmic losses increase with increasing current density.

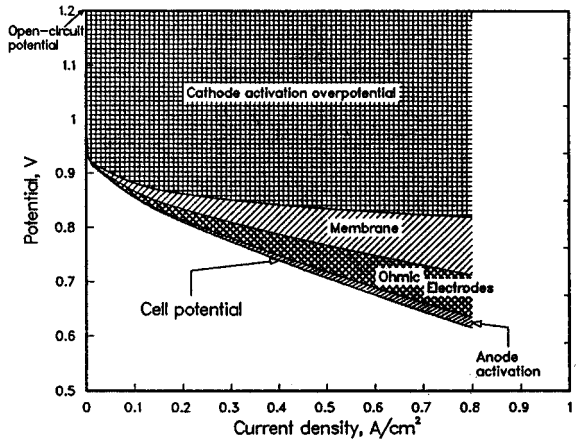

Fig. 12: Model calculations of the contributions to PEMFC losses as a function of current density with no mass transport limitation[82].

A balance between model accuracy and calculation time is usually maintained by a number of assumptions, e.g. 1D geometry, isothermal conditions, fully hydrated conditions, steady state operation and material homogeneity. Relaxation of these assumptions leads to increasing model complexity and requires a more detailed physical model, particularly in the porous active layer. In recent years, much effort has been devoted to the simplified description of the complex structure of this region. A typical active layer consists of ~ 300 nm agglomerates of ~ 30 nm carbon particles with 2 – 3 nm Pt particles supported on them. This porous structure has a bimodal pore size distribution, with smaller (20 – 40 nm) pores between carbon particles and larger (40 – 200 nm) pores between the agglomerates. Simplified models of this structure have been proposed using spherical[83], slab[84] and cylindrical[85] agglomerates. Modelling of two phase flow[86] and water management[87] has also attracted attention in recent years. Modelling of flow field patterns is an important design tool for bipolar plate manufacturers[88]. 3D models[89,90] to describe the complete operation of the PEMFC have started to appear in the literature. However, a detailed theoretical treatment of the various models in the literature is beyond the scope of this review.

3 DURABLITY OF PEM FUEL CELLS

There has been an increased interest in recent years in the study of degradation processes in PEM fuel cells. This has been driven by the need to ensure stability and reliability of performance in service as the timescale for commercialisation of the technology continues to decrease. Fuel cell lifetime requirements vary from 4000 h for car applications up to 20,000 h for buses and 40,000 h for stationary applications. Degradation rate limits are usually set based on beginning-of-life (BOL) and end-of-life (EOL) performance specifications and are typically in the range 1-10 μV/h. A number of individual well-engineered PEMFC stacks, e.g. from Ballard, have already been demonstrated to satisfy these requirements, but in most cases there is a need to improve the long term performance. At present, the fuel cell industry cannot guarantee the above lifetimes under anything but the most benign and stable service conditions. The physical mechanisms of fuel cell degradation are not well understood but qualitatively are a result of irreversible changes in the kinetic and/or transport properties of the cell. Recent reviews of the subject have been conducted by Gottesfeld and Zawodzinski[91] and Fowler et al[92]. While the performance of fuel cells at BOL is relatively well understood, there has been very little EOL analysis of PEMFC stacks. Post mortem analysis of materials and components and modelling of performance degradation are required to enhance understanding of these processes. Degradation of PEMFC performance is unavoidable; the aim of the designer should be to minimise the rate of degradation.

A summary of the major failure modes and their likely causes is presented in Table 1. In most cases a combination of the inherent reactivity of component materials, harsh operating conditions, contamination and poor design/assembly is responsible for the onset of degradation.

The principal indicator of fuel cell durability is conventionally taken to be the voltage decay rate, usually expressed in μV/h. The results of a selection of PEMFC durability tests from the literature are shown in Table 2. Direct comparison is difficult as the details of operating history and experimental conditions are not usually specified. In many of these tests, simulated reformate was used rather than pure hydrogen to reflect service conditions more accurately. It must be emphasised that most long term durability tests evaluate the stability of cell performance under steady load. When the fuel cell is subjected to more demanding conditions, such as fluctuating loads, freeze/thaw cycles and shut down/start up, the observed degradation rates are significantly higher than those in Table 2. This is illustrated by Fowler et al[93], who reported an overall voltage decay rate of 120 μV/h for a PEMFC that had been used by their group for 10 years with approximately 600 h of non-continuous operation under a variety of conditions, including stop-start cycling, long term storage, dehydration and flooding.

Table 1: Summary of major failure modes in PEM fuel cells.

Component	Failure modes	Causes
Membrane	Chemical attack	Contamination Non-uniform distribution of reactants/water/coolant Mechanical stress
	Conductivity loss	Drying of membrane Contamination
	Delamination from electrode	Thermal/mechanical stress
Active layer	Loss of activation	Sintering of electrocatalyst Corrosion of electrocatalyst Poisoning
	Decrease in mass transport rate of reactants	Mechanical stress Contamination
	Loss of reformate tolerance	Dealloying of electrocatalyst
	Decrease in control of water management	Change in hydrophobicity of materials
GDL	Decrease in mass transport rate of reactants	Degradation of backing material Mechanical stress
	Conductivity loss	Corrosion
	Decrease in control of water management	Change in hydrophobicity of materials
Bipolar plate	Conductivity loss	Corrosion
	Fracture/deformation	Mechanical stress
Gasket	Mechanical failure	Corrosion Mechanical stress

Table 2: Results of long term durability tests under laboratory conditions.

Authors	Test time	Degradation rate
Ralph[94] 1996	5000 h	4 μV/h
Sishtla et al[95] 1998	5100 h	6 μV/h
Washington[96] 2000	4700 h 8000 h	6 μV/h 2.2 μV/h
Nakayama[97] 2000	4000 h	4.3 μV/h
Isono et al[98] 2000	2000 h	10 μV/h
Maeda et al[99] 2000	5000 h	6 μV/h
Endoh et al[100] 2002	4000 h	2 μV/h
Knights et al[101] 2004	12000 h	0.5 μV/h
Cheng et al[102] 2004	4000 h	3.1 μV/h
Scholta et al[103] 2004	2500 h	20 μV/h

Apart from membrane pinhole formation, which is catastrophic in terms of cell operation, all of the other degradation modes listed in Table 1 contribute in some way to a gradual decay of cell voltage with time. Contamination of the MEA by impurities leached from the fuel cell components or introduced through the reactant gases is a major cause of degradation. The anode gas may contain impurities from the reforming process, while systems operating in urban environments may be forced to operate on air containing pollutants such as NO_x, SO_2 and dust particles. Poor water management is another major factor contributing to degradation. If the humidity is too low, the membrane will dry out, leading to increased ohmic losses, while if it is too high, flooding will lead to increased mass transport losses, particularly at the cathode. The maintenance of an optimum humidity level and temperature over the entire area of each membrane in a fuel cell stack is a challenge, particularly with fluctuating loads, where the response of the humidification system is often too slow to keep pace with

the load following characteristics of the fuel cell. In general, the maintenance of uniform, steady conditions in the cell is conducive to good long term performance. Degradation of the various fuel cell components is discussed in more detail below.

Electrocatalyst

Changes in the structure, chemistry and distribution of the electrocatalyst over time can lead to an increase in activation losses and therefore a decrease in cell performance. In particular, loss of surface area may occur due to sintering and/or oxidation of electrocatalyst particles. Loss of Pt surface area proceeds through electrodissolution/re-deposition and surface migration of Pt atoms, with the driving force being the minimisation of surface energy. Similar phenomena have been observed for Pt electrocatalysts in phosphoric acid fuel cells[104]. The mobility of platinum has been demonstrated on bulk platinum[105], on highly oriented pyrolytic graphite[106] and on carbon-supported PEMFC electrocatalysts[107,108]. The evolution of electrocatalyst microstructure with time was monitored by Cheng et al[109], using XRD, TEM and Raman spectroscopy. The particle size of the carbon-supported electrocatalyst on both anode (PtRu) and cathode (Pt) was observed to increase with time as shown in Table 3. The concentration of RuO_2 at the anode was found to increase with time, but no oxides were identified at the cathode.

Table 3: Average particle size (nm) of electrocatalysts as a function of exposure time in a PEMFC, calculated from XRD by the full width half maximum (fwhm) and Laue integration width methods[110].

	fwhm		**Laue**	
Time (h)	**Anode**	**Cathode**	**Anode**	**Cathode**
0	3.2	5.0	3.3	5.0
200	3.2	5.6	3.3	5.4
500	4.6	6.3	3.6	5.2
700	5.4	8.1	5.2	7.5
1000	5.8	6.9	4.0	5.8

Schulze et al[111] examined MEAs using XPS and EDX after several days operation at 0.5 V. They observed a dramatic decrease in Pt concentration in the XPS spectra at the anode surface, while that at the cathode remained unchanged. The cell performance was unaffected. This was explained by a redistribution of the electrocatalyst into larger three dimensional structures, which leads to a reduction in the XPS signal. In a separate experiment, accumulation of platinum in the cathode active layer was observed by EDX. When this experiment was repeated in a segmented cell with some flooded anode segments, the accumulation of Pt was only observed opposite to the flooded segments and not opposite the dry anode segments.

Large particles of platinum oxide (~50 μm) were also identified on the outside of the cathode GDL. These results demonstrate that the movement of platinum is supported by the presence of liquid water. St-Pierre et al also noted that the hydration level will have an effect on particle growth in the electrocatalyst[112]. Gulzow et al observed migration of Pt into the interface between the anode and the membrane[113].In some cases, no deterioration in cell performance is observed despite evidence of catalyst sintering. This may be due to the particle size effect, whereby the decrease in surface area is compensated by a higher activity per unit surface area[114].

In fuel cell stacks, non-uniform distribution of reactant gases between cells can result in partial or complete fuel and/or oxidant starvation in individual cells. This is of particular concern during start up at sub-zero temperatures, where ice can block the flow channels. Rapid heating of the stack at start up is advisable to avoid this scenario. Under conditions of oxidant starvation, the cell acts as a hydrogen pump, with H^+ ions combining to form hydrogen at the cathode in the absence of oxygen. The cell potential drops almost to zero and may even become negative. Fuel starvation is more detrimental to long term performance, since oxidation of water occurs in the absence of hydrogen and the anode potential rises to that required to oxidise water (> 1.23 V). This high potential leads to corrosion of both electrocatalyst and carbon support, resulting in a loss of activity. Such degradation can be reduced by modification of the anode structure to favour oxidation of water over carbon[115].

The effect of cell reversal on the electrocatalyst during fuel starvation was investigated by Taniguchi et al[116]. Ru dissolution from individual electrocatalyst particles was identified at the anode, while loss of Pt surface area at the cathode was also observed. The extent of Ru dissolution at the anode was greatest near the fuel outlet. At the cathode, the mean Pt particle diameter increased from 2.64 nm to 4.95 nm during the test. This increase in particle size was correlated with a decrease in active surface area of the cathode of around 28%, as determined from hydrogen adsorption.

Ahn et al conducted a post mortem analysis of a 2.63 kW PEMFC stack after 1800 h operation using electron microscopy, cyclic voltammetry, impedance spectroscopy and X-ray fluorescence spectroscopy[117]. They found a decrease in active surface area of 23% from hydrogen adsorption and an increase in charge transfer resistance by a factor of 5.8 from impedance spectroscopy. A rapid decay in performance was observed during the test. The failure of the cell was ascribed to degradation of the catalyst and contamination of the MEA.

The effect of sub-zero operating temperatures on cell durability has been studied by a number of authors. Kagami et al[118] found that the voltage decay rate was significant when operating below 0 °C. The rate of decay was accelerated by increasing the current density. Cho et al investigated the effect of freeze/thaw cycling on the performance of a PEMFC and found that the performance degraded after each cycle. This was ascribed to increases in charge transfer and contact resistances and a decrease in active surface area[119]. Two methods of mitigation were proposed by Cho

et al[120]; gas-purging of the flow channels and solution-purging with antifreeze. Both methods were successful in reducing the degradation rate.

Endoh et al detected carbon radicals in the active layers of degraded MEAs using electron spin resonance[121]. The authors suggested that these radicals were generated by a reaction between the carbon support and either or both of the hydroxyl or hydroperoxyl radicals from the membrane.

Surface oxidation of Pt has also been reported to decrease the electrocatalytic activity for oxygen reduction[122]. Using cyclic voltammetry, Paik et al measured the extent of oxidation of Pt electrocatalysts in a PEMFC as a function of O_2 concentration at the cathode[123]. At 0.85 V, the formation of platinum oxide was proportional to O_2 concentration at constant exposure time, while at 0.95 V, no such dependence was observed.

Poisoning of the anode electrocatalyst surface by adsorbed CO has been extensively studied. However, the effect of CO is reversible and may be mitigated by purging with an inert gas or by air bleed and this review is concerned only with irreversible performance degradation.

Membrane

Nafion-type membranes have proved extremely stable for applications such as ion exchange and electrolysis, with lifetimes of tens of thousands of hours, but they are far more susceptible to degradation when placed in the harsh environment of a PEMFC. Membrane lifetime is generally the most severe limitation on PEMFC durability under service conditions. Chemical attack of the membrane by contaminants is a major source of degradation. These contaminants may originate from corrosion of the bipolar plates[124] or electrodes[125]. Ma et al postulated that such contaminants disable proton conductivity sites in the membrane, leading to a decrease in conductivity over time[126]. The accepted chemical degradation mechanism for Nafion membranes is peroxide radical attack catalysed by metal ions[127]. The strongest evidence for this mechanism is the presence of hydrogen peroxide in the product water. It is possible that different membrane degradation mechanisms are in operation close to the cathode and anode. Panchenko et al have designed an experimental PEMFC capable of in-situ EPR analysis of organic radicals in the membrane[128], although to date they have not reported any results. Bosnjakovic and Schlick also used EPR spectroscopy to monitor the concentration of intermediate radicals during the treatment of Nafion membranes with Fenton reagent[129].

Huang et al[130] used XRD and XPS to investigate the degradation of Nafion membranes due to PEMFC operation. XRD showed that low gas humidification caused a decrease in the degree of crystallinity of the Nafion, as well as that of the electrocatalyst and carbon support. From the XPS spectra, the authors deduced that

the Nafion had decomposed during fuel cell operation, close to the anode in particular. They concluded that degradation of the membrane proceeds through hydrogen reacting with CF_n groups in the hydrophobic phase of Nafion under the anode potential.

Yu et al[131] studied the degradation of a polystyrene sulphonic acid (PSSA) membrane using EDX and IR spectroscopy. They concluded that peroxide intermediates at the cathode attack the tertiary hydrogen at the α-carbon of the PSSA, leading to decomposition of the membrane. They demonstrated the improved stability of Nafion-PSSA composite membranes.

Another important factor in the durability of the membrane is its mechanical strength. Wakizoe et al showed that a reinforced membrane performed better under start-stop cycling than an unreinforced membrane[132], while Cleghorn also emphasised the importance of dimensional stability of the membrane[133]. It is generally accepted that degradation of the membrane is enhanced by mechanical stress[134], which is exacerbated by misalignment of components and/or unnecessarily high compressive forces.

Poor water management can also accelerate membrane degradation. Although a temporary drop in performance due to membrane dehydration can usually be recovered by humidification, if the membrane is operating in dehydrated condition for an extended period failure due to reactant crossover can occur. In general, the drier the conditions, the shorter the lifetime of the cell. A combination of low humidification and uneven distribution of reactant will lead to local hotspots, which are very prone to membrane failure.

Bipolar plates

Corrosion of bipolar plates has two adverse effects on fuel cell durability; contamination of the fuel cell with corrosion product and an increase in contact resistance. The impact of the former is most severe on the membrane, where the accepted major degradation mechanism is peroxide radical attack catalysed by metal ions[135]. The latter is caused by the formation of a resistive surface film (such as a passive layer on stainless steel) and results in increased ohmic losses. It is therefore imperative that bipolar plate materials with good corrosion resistance are used, although a balance is still required between cost, performance and durability. Other desirable properties in a bipolar plate are low resistivity (including contact resistance), high mechanical strength, low density, low reactivity, impermeability to reactant gases and low cost (both in terms of raw material and processing). The suitability of a variety of stainless steels was discussed by Davies et al, who showed that the thickness and resistivity of passive films varies with the type of alloy used[136].

Another common problem is fracture or deformation of bipolar plates under the compressive forces used to endure adequate sealing and good electrical contact. Thermal cycling may reduce the mechanical strength of these materials. In general, stainless steel performs better than graphitic materials in this regard, although composite materials are still under development.

Gaskets

Schulze et al highlighted the problem of degradation of sealing materials during fuel cell operation[137]. Typical gasket materials are fluorine caoutchouc, EPDM and silicone. Poor sealing results in fuel losses and a reduced voltage due to a mixed potential at the electrodes. Using XPS, the authors found traces of silicone in the anode and electrocatalyst layers but not within the membrane. They suggested that the accumulation of silicone in these areas could disturb the wetting character of the electrodes, the water balance of the cell and react with the electrocatalyst at the cathode. Migration of Si into both membrane and electrode was also observed by Ahn et al[138].

Models

Very little modelling of PEMFC degradation has been carried out to date. One of the few papers on the subject was recently published by Kulikovsky et al[139], who demonstrated that cell voltage decay could be represented by a degradation wave propagating along the cathode channel towards the outlet. The model assumes that local degradation is initiated above a certain threshold current density, after which the local current is interrupted. This forces the current density in adjacent areas to increase, leading to a degradation wave front, behind which the performance is zero and ahead of which the mean current density is increasing with time to support the constant total current. No attempt was made to model the actual physical mechanism of degradation.

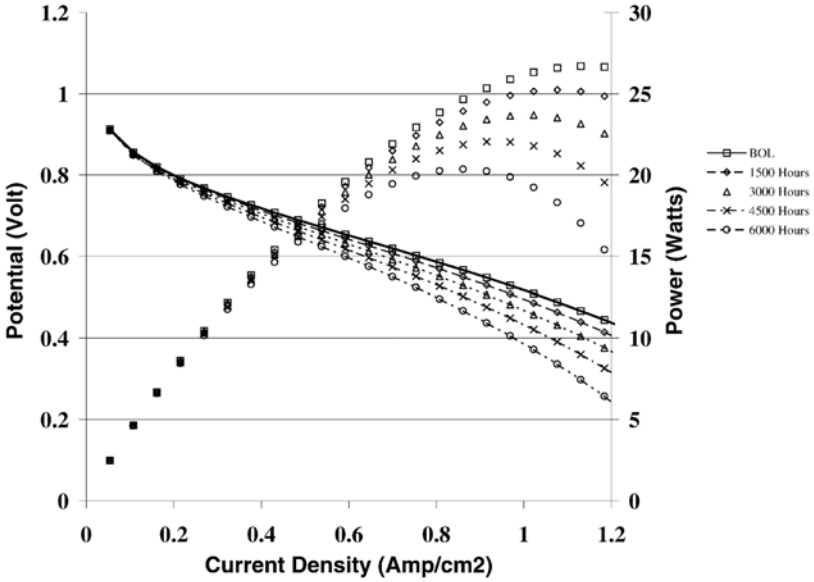

Fig. 13: Simulation of cell ageing using the model of Fowler et al[140].

Fowler et al modified their performance model[141] to include semi-empirical time-dependent parameters to account for ageing of the cell[142]. Three terms are added. The first term accounts for the deterioration in membrane conductivity, the second term represents the decay of electrocatalyst activity with time and the third term deals with the decrease in the rate of mass transport within the MEA. The model is capable of predicting changes in experimental polarisation curves with time due to these degradation processes, as illustrated in Fig. 13.

4 KEY ISSUES

As commercialisation of fuel cell technology moves closer to reality, robust test techniques and protocols will be required to ensure durability and reliability of performance under service conditions. At present PEM fuel cells have been demonstrated to provide stable performance under steady load for lifetimes of tens of thousands of hours, but their performance under more representative service conditions, i.e. stop/start cycling, thermal cycling, variable load and abusive handling, does not satisfy acceptable long term performance criteria. Improvements in existing test techniques and development of novel measurement techniques are required to improve understanding of degradation processes, inform designers and users about best practice and provide diagnostic tools for failure analysis. The industry would then be in a better position to give clear specifications to a supply chain that currently does not fully exist.

The development of reliable in-situ techniques for monitoring variables such as temperature, humidity, water handling and concentration of contaminants would provide important feedback to stack and component manufacturers. More detailed information on the spatial distribution of these parameters would allow designers to optimise material properties and stack design to prolong fuel cell life without compromising performance. A major industry requirement is the development of rapid diagnostic tests capable of isolating potential problems as early as possible in the product cycle. From a technical perspective, the following developments are required:

- Local temperature/humidity mapping
- Modelling/measurement of two phase flow
- Development of in-situ reference electrode
- In-situ evaluation of membrane degradation
- Corrosion testing of fuel cell components
- Characterisation of catalyst layer processes on nanoscale
- Impedance spectroscopy as a reliable diagnostic tool
- In-situ contaminant monitoring in reactant gases
- Ex-situ MEA quality control test
- Accelerated ageing tests

In-situ temperature mapping offers a potentially viable method for testing of the system whilst detecting hotspots, which are often a significant limiting factor in the lifetime of the membrane. The measurement of humidity and temperature on a local scale could be carried out using microprobes, such as very fine thermocouples, thermometers or optical fibres. Mapping of the spatial distribution of temperature and humidity would allow fuel cell designers to tailor the water handling properties of the fuel cell materials to trap/move water in particular locations as required. In-situ monitoring of contaminants in both hydrogen and air feeds would be beneficial, since the purity of incoming gas is critical to fuel cell performance. A highly instrumented cell would be required. Alternatively, a standard three electrode cell could be used, with the contaminants being introduced into the liquid phase. Techniques for the

analysis of trace elements could be applied to this type of testing. An in-situ peroxide or fluoride sensor could be developed to monitor degradation of the membrane. The development of a rapid quality control test would obviate the need to test every MEA in a stack. The establishment of a reliable reference electrode for PEM fuel cells is a key goal, particularly in systems fed on reformate, where the polarisation of each electrode is comparable. The development of a reference electrode that could measure the polarisation of both anode and cathode would open up the characterisation of the fuel cell using a whole range of electrochemical techniques.

A fundamental requirement is the development of tools to understand and improve the action of electrocatalysts at the atomic scale, using modelling and validation of models through novel measurement techniques. It may be that characterisation of water on the nanoscale could be an intermediate step in the characterisation of catalyst activity. Fuel cell developers need to know which parts of the catalyst layer are most electrochemically active in order to maximise the density of active sites within the layer. Heterogeneity within active layers on the nanoscale is an important processing issue. Modelling of two phase flow where the water and gas are moving in opposite directions is particularly challenging. There is a need to extract the effect of processing method on catalyst activity, since nominally similar catalysts may show quite differing performance when tested. Techniques to map the performance of individual catalyst particles would be useful in this context. Microcapillary techniques are a possibility, but the resolution would probably not be adequate. Another option would be to map the active sites by replacing the hydrogen with tritium.

Improved understanding of degradation mechanisms is critical to the development of more efficient and reliable fuel cells. A useful experimental approach here would be to test fuel cells under conditions designed to accelerate one particular mode of degradation and to look for correlation between material properties and cell performance over time. Such an approach should be adopted in the testing stage of this project. Given the three year timescale of the project and the fact that the test rig can accommodate only one MEA for test times of order 1000 h, it is necessary to design a test schedule that maximises the information obtainable from a small matrix of test conditions.

Two sets of test conditions are proposed for the study of PEMFC degradation in this project:

1. Harsh: non-humidified cell.
2. Mild: fully-humidified cell.

In-situ and post-mortem tests would correlate the effects of the harsh test on the fuel cell materials and components, using the mild test as a benchmark. The use of reformate is probably not feasible given the timescale and issues with polarisation of the anode. A second variable would be the mode of operation, i.e. steady load vs stop/start. In Japan two cycles per day is the norm, with short on-load times. This would give a 2 x 2 matrix of test conditions, as shown in Table 4. The use of uninterrupted power supply (UPS) is necessary for such long term tests and any required shutdown should be carried out under controlled conditions to avoid damage to the cell at this point.

Table 4: Proposed testing matrix.

	Steady load	**Stop/start**
Humidified	1	2
Dry	3	4

5 SUMMARY

PEM fuel cell performance may be characterised using a combination of electrochemical techniques, structural characterisation and chemical analysis. A variety of different models have been developed to describe the performance of such cells as a function of their fabrication method and operating conditions. Long term performance and durability of PEM fuel cells are of increasing importance as commercialisation of the technology gathers pace. While performance at beginning of life is relatively well characterised, very little systematic work on PEMFC durability has been reported to date in the literature. There is a need to apply the full range of diagnostic techniques, including modelling, to the study of PEMFC degradation in order to better inform designers and manufacturers of fuel cells and to guide best practice during fuel cell operation.

ACKNOWLEDGEMENTS

This work was conducted as part of the Materials Performance programme, a joint venture between the United Kingdom Department of Trade and Industry and an Industrial Advisory Group comprising C Tech Innovation, Fuel Cell Control, Ineos Chlor, Intelligent Energy, Johnson Matthey and Morgan Fuel Cell.

REFERENCES

[1] Reprinted with permission from D.M. Bernardi, M.W. Verbrugge, Proc. of the Symposium on Modeling of Batteries and Fuel Cells, 1991, Phoenix, U.S.A., p.240. Copyright 1991, The Electrochemical Society.

[2] S.K.A. Wasmus, J. Electroanal. Chem., **461**, 14 (1999).

[3] V. Mehta, J.S. Cooper, J. Power Sources, **114**, 32 (2003).

[4] Y.G. Chun, C.S. Kim, D.H. Peck, D.R. Shin, J. Power Sources, **71**, 174 (1998).

[5] A. Fischer, J. Jindra, H. Wendt, J. Applied Electrochem., **28**, 277 (1998).

[6] M.S. Wilson, S. Gottesfeld, J. Electrochem. Soc., **139**, L28 (1992).

[7] M.S. Wilson, S. Gottesfeld, J. Applied Electrochem., **22**, 1 (1992).

[8] M. Uchida, Y. Aoyama, N. Eda, A. Ohta, J. Electrochem. Soc., **142**, 4143 (1995).

[9] N. Jia, R.B. Martin, Z. Qi, M.C. Lefebvre, P.G. Pickup, Electrochim. Acta, **43**, 3665 (2001).

[10] E. Passalacqua, F. Lufrano, G. Squadrito, A. Patti, L. Giorgi, Electrochim. Acta, **46**, 799 (2001).

[11] V.A. Paganin, E.A. Ticianelli, E.R. Gonzalez, J. Appl. Electrochem., **26**, 297 (1996).

[12] D.H. Peck, Y.G. Chun, C.S. Kim, D.H. Jun, D.R. Shin, J. New Mat. Electrochem. Systems, **2**, 121 (1999).

[13] J.M. Song, S.Y. Cha, W.M. Lee, J. Power Sources, **94**, 78 (2001).

[14] S.J. Lee, S. Mukerjee, J. McBreen, Y.W. Rho, Y.T. Kho, T.H. Lee, Electrochim. Acta, **42**, 3693 (1998).

[15] A. Fischer, H. Wendt, Proc. Fuel Cell Seminar 1996, Orlando, U.S.A., p. 579.

[16] S.F. Simpson, C.E. Salinas, A.J. Cisar, O.J. Murphy, Proceedings of the First International Symposium on Proton Conducting Membrane Fuel Cells, 1995, Chicago, U.S.A., p.182.

[17] P.-W. Li, T. Zhang, Q.-M Wang, L. Schaefer, M.K. Chyu, J. Power Sources, **114**, 63 (2003).

[18] P. Adcock, P. Mitchell, J. Moore, Proc. Fuel Cell Seminar 1996, San Diego, U.S.A., p. 30.

[19] S.J.C. Cleghorn, C.R. Derouin, M.S. Wilson, S. Gottesfeld, J. Appl. Electrochem., **28**, 663 (1998).

[20] M. Noponen, J. Ihonen, A. Lundblad, G. Lindbergh, J. Appl. Electrochem., **34**, 255 (2004).

[21] Reprinted from M. Noponen, J. Ihonen, A. Lundblad, G. Lindbergh, J. Appl. Electrochem., **34**, 255 (2004) with the permission of Kluwer.

[22] M.M. Mench, C.Y. Wang, J. Electrochem. Soc., **150**, A79 (2003).

[23] A. Hakenjos, H. Muenter, U. Wittstadt, C. Hebling, J. Power Sources, **131**, 213 (2004).

[24] A.B. Geiger, R. Eckl, A. Wokaun, G.G. Scherer, J. Electrochem. Soc., **151**, A394 (2004).

[25] C. Wieser, A. Helmbold, E. Gulzow, J. Appl. Electrochem., **30**, 803 (2000).

[26] J.R. Claycomb, A. Brazdeikis, M. Le, R.A. Yarbrough, G. Gogoshin, J.H. Miller, IEEE Trans. Appl. Supercond., **13**, 211 (2003).

[27] Reprinted with permission from D.A. Stevens, J.R. Dahn, J. Electrochem. Soc., **150**, A770 (2003). Copyright 2003, The Electrochemical Society.

[28] T. Biegler, D.A.J. Rand, R. Woods, J. Electroanal. Chem., **29**, 269 (1971).
[29] A. Essalik, K. Amouzegar, O. Savadogo, J. Appl. Electrochem., **25**, 404 (1995).
[30] A. Parthasarathay, S. Srinivasan, A.J. Appleby, C.R. Martin, J. Electroanal. Chem., **339**, 101 (1992).
[31] H. Gasteiger, N. Markovic, P.N. Ross, J. Phys. Chem., **99**, 8290 (1995).
[32] D.A. Stevens, J.R. Dahn, J. Electrochem. Soc., **150**, A770 (2003).
[33] F. Gloaguen, F. Andolfatto, R. Durand, P. Ozil, J. Appl. Electrochem., 24, 863 (1994).
[34] A. Parthasarathay, C.R. Martin, S. Srinivasan, J. Electrochem. Soc., **138**, 916 (1991).
[35] F. Uribe, T.E. Springer, S. Gottesfeld, J. Electrochem. Soc., **139**, 765 (1992).
[36] R. O'Hayre, F.B. Prinz, J. Electrochem. Soc., **151**, A756 (2004).
[37] R.L. Borup, N.E. Vanderborgh, Mat. Res. Soc. Symp. Proc., **393**, 151 (1995).
[38] M. Li, S. Luo, C. Zeng, J. Shen, H. Lin, C. Cao, Corros. Sci., **46**, 1369 (2004).
[39] W.J. Wruck, R.M. Machado, T.W. Chapman, J. Electrochem. Soc., **134**, 539 (1987).
[40] F.N. Buchi, A. Marek, G.G. Scherer, J. Electrochem. Soc., **142**, 1895 (1995).
[41] Reprinted from T. Mennola, M. Mikkola, M. Noponen, T. Hottinen, P. Lund, J. Power Sources, **112**, 261 (2002) with permission from Elsevier.
[42] G.G. Scherer, A. Marek, Res. Report CRB 87-41 C, Brown Boveri Research Center, Switzerland (1987).
[43] T. Mennola, M. Mikkola, M. Noponen, T. Hottinen, P. Lund, J. Power Sources, **112**, 261 (2002).
[44] F. Jaouen, G. Lindbergh, J. Electrochem. Soc., **150**, A1711 (2003).
[45] F. Jaouen, G. Lindbergh, J. Electrochem. Soc., **150**, A1699 (2003).
[46] Reprinted from T. Mennola, M. Mikkola, M. Noponen, T. Hottinen, P. Lund, J. Power Sources, **112**, 261 (2002) with permission from Elsevier.
[47] T. Abe, H. Shima, K. Watanabe, Y. Ito, J. Electrochem. Soc., **151**, A101 (2004).
[48] Reprinted with permission from F. Jaouen, G. Lindbergh, J. Electrochem. Soc., **150**, A1711 (2003). Copyright 2003, The Electrochemical Society.
[49] Reprinted from P. Kurzweil, H.-J. Fischle, J. Power Sources, **127**, 331 (2004) with permission from Elsevier.
[50] T.E. Springer, T.A. Zawodzinski, M.S. Wilson, S. Gottesfeld, Proc. First International Symposium on Proton Conducting Membrane Fuel Cells, Chicago, U.S.A., p.137.
[51] M.C. Lefebvre, R.B. Martin, P.G. Pickup, Electrochem. Solid State Lett., **2**, 259 (1999).
[52] C.A. Schiller, F. Richter, E. Gulzow, N. Wagner, Phys. Chem. Chem. Phys., **3**, 374 (2001).
[53] M. Ciureanu, H. Wang, J. Electrochem. Soc., **146**, 4031 (1999).
[54] N. Wagner, E. Gulzow, J. Power Sources, **127**, 341 (2004).
[55] B. Andreaus, A.J. McEvoy, G.G. Scherer, Electrochim. Acta, **47**, 2223 (2002).
[56] T. Romero-Castanon, L.G. Arriaga, U. Cano-Castillo, J. Power Sources, 118, 179 (2003).
[57] L.J. van der Pauw, Philips Res. Repts., **13**, 1 (1958).
[58] M. Fowler, J.C. Amphlett, R.F. Mann, B.A. Peppley, P.R. Roberge, J. New Mat. Electrochem. Systems, **5**, 255 (2002).
[59] S.H. Kwak, D.H. Peck, Y.G. Chun, C.S. Kim, K.H. Yun, J. New Mat.

Electrochem. Systems, **4**, 25 (2001).

[60] A. Lundblad, J. New Mat. Electrochem. Systems, **7**, 21-28 (2004).

[61] Reprinted with permission from H. Kim, B. Popov, Electrochem. Solid State Lett., **7**, A71 (2004). Copyright 2004, The Electrochemical Society.

[62] Reprinted from J.H. Tian, F.B. Wang, Z.Q. Shan, R.J. Wang, J.Y. Zhang, J. Appl. Electrochem., **34**, 461, 2004 with permission from Kluwer.

[63] A. Fischer, J. Jindra, H. Wendt, J. Applied Electrochem., **28**, 277 (1998).

[64] P.A. Webb, C. Orr, Analytical Methods in Fine Particle Technology, Micrometrics Instrument Corporation, p. 155, 1997.

[65] M. Watanabe, M. Tomikawa, S. Motoo, J. Electroanal. Chem., **195**, 81 (1985).

[66] M. Uchida, Y. Aoyama, N. Eda, A. Ohta, J. Electrochem. Soc., **142**, 4143 (1995).

[67] M. Uchida, Y. Fukuoka, Y. Sugawara, N. Eda, A. Ohta, Proc. Fuel Cell Seminar 1996, Orlando, U.S.A., p. 612.

[68] A. Lundblad, J. New Mat. Electrochem. Systems, **7**, 21-28 (2004).

[69] S. Gamburzev, A.J. Appleby, J. Power Sources, **107**, 5 (2002).

[70] Reprinted from P. Gode, F. Jaouen, G. Lindbergh, A. Lundblad, G. Sundholm, Electrochim. Acta, **48**, 4175 (2003) with permission from Elsevier.

[71] P. Gode, F. Jaouen, G. Lindbergh, A. Lundblad, G. Sundholm, Electrochim. Acta, **48**, 4175 (2003).

[72] F. Jaouen, G. Lindbergh, G. Sundholm, J. Electrochem. Soc., **149**, A437 (2002).

[73] M. Prasanna, H.Y. Ha, E.A. Cho, S.-A. Hong, I.-H. Oh, J. Power Sources, 131, 147 (2004).

[74] H.-S. Chu, C. Yeh, F. Chen, J. Power Sources, **123**, 1 (2003).

[75] M. Schulze, N. Wagner, G. Steinhilber, E. Gulzow, M. Wohr, K. Bolwin, Proc. Fuel Cell Seminar 1996, Orlando, U.S.A., p. 663.

[76] J. Kim, S.-M. Lee, S. Srinivasan, J. Electrochem. Soc., **142**, 2670 (1995).

[77] J.C. Amphlett, R.M. Baumert, R.F. Mann, B.A. Peppley, P.R. Roberge, Proc. 28th Intersociety Energy Conversion Engineering Conference, Washington D.C., U.S.A., 1993, p. 1215.

[78] L. Pisani, G. Murgia, M. Valentini, B. D'Aguanno, J. Power Sources, **108**, 192 (2002).

[79] W.-Y. Lee, G.-G. Park, T.-H. Yang, Y.-G. Yoon, C.-S. Kim, Int. J. Hydrogen Energy, **29**, 961 (2004).

[80] T.E. Springer, M.S. Wilson, S. Gottesfeld, J. Electrochem. Soc., **140**, 3513 (1993).

[81] D.M. Bernardi, M.W. Verbrugge, Proc. of the Symposium on Modeling of Batteries and Fuel Cells, 1991, Phoenix, U.S.A., p.240.

[82] Reprinted with permission from D.M. Bernardi, M.W. Verbrugge, Proc. of the Symposium on Modeling of Batteries and Fuel Cells, 1991, Phoenix, U.S.A., p.240. Copyright 1991, The Electrochemical Society.

[83] M.L. Perry, J. Newman, E.J. Cairns, J. Electrochem. Soc., **145**, 5 (1998).

[84] F. Gloaguen, P. Convert, S. Gamburzev, O.A. Velev, S. Srinivasan, Electrochim. Acta, **43**, 3767 (1998).

[85] L. Pisani, G. Murgia, M. Valentini, B. D'Aguanno, J. Electrochem. Soc., **149**, A898 (2002).

[86] L. You, H. Liu, Int. J. Heat and Mass Transfer, **45**, 2277 (2002).

[87] P. Berg, K. Promislow, J. St. Pierre, J. Stumper, B. Wetton, J. Electrochem. Soc., **151**, A341 (2004).

[88] P.-W. Li, L. Schaefer, Q.-M. Wang, T. Zhang, M.K. Chyu, J. Power Sources, **115**,

90 (2003).
[89] S. Mazumder, J.V. Cole, J. Electrochem. Soc., **150**, A1503 (2003).
[90] S. Um, C.Y. Wang, J. Power Sources, **125**, 40 (2004).
[91] S. Gottesfeld, T.A. Zawodzinski, Polymer electrolyte fuel cells, in: R.C. Alkire, H. Gerischer, D.M. Kolb, C.W. Tobias (Eds.), Advances in Electrochemical Science and Engineering, vol. 5, Wiley-VCH, Weinheim, 1997, p. 195.
[92] M. Fowler, J.C. Amphlett, R.F. Mann, B.A. Peppley, P.R. Roberge, J. New Mat. Electrochem. Systems, **5**, 255 (2002).
[93] M. Fowler, J.C. Amphlett, R.F. Mann, B.A. Peppley, P.R. Roberge, J. New Mat. Electrochem. Systems, **5**, 255 (2002).
[94] T. Ralph, Platinum Metal Review, **41**, 102 (1997).
[95] C. Sishtla, G. Koncar, R. Platon, S. Gamburzev, J. Power Sources, **71**, 249 (1998).
[96] K. Washington, Proc. Fuel Cell Seminar 2000, Portland, U.S.A., p. 468.
[97] T. Nakayama, Proc. Fuel Cell Seminar 2000, Portland, U.S.A. p. 468.
[98] T. Isono, S. Suzuki, M. Kaneko, Y. Akiyama, Y. Miyake, I. Yonezu, J. Power Sources, **86**, 269 (2000).
[99] H. Maeda, A. Yoshimura, H. Fukumoto, Proc. Fuel Cell Seminar 2000, Portland, U.S.A., p. 379.
[100] E. Endoh, S. Terazono, H. Widjaja, Abstract 89, The Electrochemical Society Meeting Abstracts, Salt Lake City, U.S.A., 2002.
[101] S.D. Knights, K.M. Colbow, J. St-Pierre, D.P. Wilkinson, J. Power Sources, **127**, 127 (2004).
[102] X. Cheng, L. Chen, C. Peng, Z. Chen, Y. Zhang, Q. Fan, J. Electrochem. Soc., **151**, A48 (2004).
[103] J. Scholta, N. Berg, P. Wilde, L. Jorissen, J. Garche, J. Power Sources, **127**, 206 (2004).
[104] P. Stonehart, P.A. Zucks, Electrochim. Acta, **17**, 2333 (1972).
[105] M. Giesen, M. Dietterle, D. Stabel, H. Ibach, D. Kolb, Surf. Sci., **384**,, 168 (1997).
[106] C. Alonso, R.C. Salvarezza, J.M. Vara, A.J. Arvia, L. Vazquez, A. Bartolome, A.M. Baro, J. Electrochem. Soc., **137**, 2161 (1990).
[107] M.S. Wilson, F.H. Garzon, K.E. Sickafus, S. Gottesfeld, J. Electrochem. Soc., **140**, 2872 (1993).
[108] P. Staiti, A.S. Arico, V. Antonucci, S. Hocevar, J. Power Sources, **70**, 91 (1998).
[109] X. Cheng, L. Chen, C. Peng, Z. Chen, Y. Zhang, Q. Fan, J. Electrochem. Soc., **151**, A48 (2004).
[110] X. Cheng, L. Chen, C. Peng, Z. Chen, Y. Zhang, Q. Fan, J. Electrochem. Soc., **151**, A48 (2004).
[111] M. Schulze, A. Schneider, E. Gulzow, J. Power Sources, **127**, 213 (2004).
[112] J. St-Pierre, D.P. Wilkinson, S. Knight, M. Bos, J. New Mat. Electrochem. Systems, **3**, 99 (2000).
[113] E. Gulzow, H. Sander, N. Wagner, M. Lorenz, A. Schneider, M. Schulze, Proc. Fuel Cell Seminar 2000, Portland, U.S.A., p. 156.
[114] T.E. Springer, M.S. Wilson, F. Garzon, T.A. Zawodzinski, S. Gottesfeld, Polymer Electrolyte Fuel Cells for Transportation Applications, Los Alamos National Laboratory, Los Alamos, U.S.A., 1993.
[115] S.D. Knights, K.M. Colbow, J. St-Pierre, D.P. Wilkinson, J. Power Sources, **127**, 127 (2004).
[116] A. Taniguchi, T. Akita, K. Yasuda, Y. Miyazaki, J. Power Sources, **130**, 42

(2004).
[117] S.-Y. Ahn, S.-J. Shin, H.Y. Ha, S.-A. Hong, Y.-C. Lee, T.W. Lim, I.-H. Oh, J. Power Sources, 106, 295 (2002).
[118] F. Kagami, T. Ogawa, Y. Hishinuma, T. Ghikahisa, Fuel Cell Seminar 2002, Palm Springs, U.S.A., p. 239.
[119] E.A. Cho, J.-J. Ko, H.-Y. Ha, S.-A. Kong, K.-Y. Lee, T.-W. Lim, I.-H Oh, J. Electrochem. Soc., **150**, A1667 (2003).
[120] E.A. Cho, J.-J. Ko, H.Y. Ha, S.-A. Hong, K.-Y Lee, T.-W. Lim, I.-H. Ho, J. Electrochem. Soc., **151**, A661 (2004).
[121] E. Endoh, S. Terazono, H. Widjaja, Y. Takimoto, Electrochem. Solid State Lett., **7**, A209 (2004).
[122] A. Damjanovic, P.G. Hudson, J. Electrochem. Soc., **135**, 2269 (1988).
[123] C.H. Paik, T.D. Jarvi, W.E. O'Grady, Electrochem. Solid State Lett., **7**, A82 (2004).
[124] M. Li, S. Luo, C. Zeng, J. Shen, H. Lin, C. Cao, Corros. Sci., **46**, 1369 (2004).
[125] E. Gulzow, M. Schulze, N. Wagner, T. Kaz, R. Reissner, G. Steinhilber, A. Schneider, J. Power Sources, **86**, 352 (2000).
[126] L. Ma, S. Warthesen, D.A. Shores, J. New Mat. Electrochem. Systems, **3**, 221 (2000).
[127] G. Hubner, E. Roduner, J. Mater. Chem., **9**, 409 (1999).
[128] A. Panchenko, H. Dilger, E. Moller, T. Sixt, E. Roduner, J. Power Sources, **127**, 325 (2004).
[129] A. Bosnjakovic, S. Schlick, J. Phys. Chem. B, **108**, 4332 (2004).
[130] C. Huang, K.S. Tan, J. Lin, K.L. Tan, Chem. Phys. Lett., **371**, 80 (2003).
[131] J. Yu, B. Yi, D. Xing, F. Liu, Z. Shao, Y. Fu, H. Zhang, Phys. Chem. Chem. Phys., **5**, 611 (2003).
[132] M. Wakizoe, H. Murata, H. Takei, Proc. Fuel Cell Seminar 2000, Portland, U.S.A., p. 487.
[133] S. Cleghorn, Proc. Fuel Cell Seminar 2000, Portland, U.S.A., p. 35.
[134] S. Stucki, G.G. Scherer, S. Schagowski, E. Fisher, J. Appl. Electrochem., **28**, 1041 (1998).
[135] G. Hubner, E. Roduner, J. Mater. Chem., **9**, 409 (1999).
[136] D.P. Davies, P.L. Adcock, M. Turpin, S.J. Rowen, J. Power Sources, **86**, 237 (2000).
[137] M. Schulze, T. Knori, A. Schneider, E. Gulzow, J. Power Sources, **127**, 222 (2004).
[138] S.-Y. Ahn, S.-J. Shin, H.Y. Ha, S.-A. Hong, Y.-C. Lee, T.W. Lim, I.-H. Oh, J. Power Sources, 106, 295 (2002).
[139] A.A. Kulikovsky, H. Scharmann, K. Wippermann, Electrochem. Commun., **6**, 75 (2004).
[140] Reprinted from M.W. Fowler, R.F. Mann, J.C. Amphlett, B.A. Peppley, P.R. Roberge, J. Power Sources, **106**, 274 (2002) with permission from Elsevier.
[141] R.F. Mann, J.C. Amphlett, M.A.I. Hopper, H.M. Jensen, B.A. Peppley, P.R. Roberge, J. Power Sources, 86, 173 (2000).
[142] M.W. Fowler, R.F. Mann, J.C. Amphlett, B.A. Peppley, P.R. Roberge, J. Power Sources, **106**, 274 (2002).